Light Scattering by Aggregate Particles

Zhangfan Xing and Martha S. Hanner

Mail Stop 183-501

Jet Propulsion Laboratory

California Institute of Technology

4800 Oak Grove Drive, Pasadena CA 91 109

Submitted to: Astrophysics & Astrophysics, Main Journal

Received:

Accepted:

Running head:

Xing & Hanner

Scattering by Aggregates

Send offprint request to: M.S. Hanner

Main journal. Section: Physical and chemical processes

Thesaurus code numbers: 02.1 6.2; 02.19.2; 07.03.1

Send proofs to: Ms. Hanner

Abstract We have investigated scattering properties of aggregates, emphasizing the size of constituent monomers comparable with the wavelength of visible light, in order to model the scattering properties of cometary dust. This has differentiated our study from previous investigations of aggregates in which the size of the monomers was much smaller than the wavelength. For aggregates, the absorption cross sections tend to have less steep slopes towards longer wavelength, typically, $C_{abs} \sim \lambda^{-1}$. Consequently aggregates of absorbing material are cooler than the individual monomers, because the aggregates radiate more efficiently in the infrared. The polarization is sensitive to the shape and size of the constituent monomers as well as to the fine structure of the aggregate. Generally aggregates of highly absorbing material produce strong positive polarization around $\theta_p = 90°$, but no negative polarization near the backward direction. In contrast, silicate aggregates are the major source of strong negative polarization at larger scattering angles. A mixture of both carbonaceous and silicate aggregates results in a polarization curve which largely matches the observed negative polarization at $\theta_p \leq 20°$ and the maximum peak around $\theta_p = 90°$ for cometary dust. The same mixture also gives a reasonable rise of the phase function toward the backward direction, which is similar to the phase function of cometary dust.

Thus, we find that aggregates with constituent monomers a few tenths of a micron in size and with intermediate porosity (≈ 0.6), similar to chondritic aggregate interplanetary dust particles, are a reasonable analog for cometary dust.

Keywords: Polarization; Scattering; Comets: General

1 Introduction

To interpret remote sensing observations of astronomical dust, including dust in comets or in the disks surrounding young stars, an understanding of the scattering properties of small particles is needed.

Comets are observed under a Variety of scattering geometries. The observed quantities include thermal emission and its spectral energy distribution, geometric albedo, phase function, and polarization. Since the dust coma is optically thin, the observed quantities can be related to particle scattering properties. The thermal emission has been used to estimate the size distribution and the rate of dust mass 10ss from the nucleus. Changes in the dust scattering properties with position in the coma are often interpreted in terms of changes in the size distribution, due to fragmentation, velocity sorting, or subli mation of volatile mantles. Such interpretation requires knowledge of basic scattering properties as a function of particle size, structure, and composition.

Natural particles often have an aggregate structure, especially those that haVC grown by coagulation (Meakin & Donn 1988, Praburam & Goree 19'35). 1'articles "grown" in the computer by diffusion limited aggregation or cluster- cluster aggregation also exhibit a porous aggregate structure (e.g. Kozasa et al. 1992, 1 993). Cometary dust particles are likely to have an aggregate structure, based 011 the morphology of interplanetary dust particles (IDPs) collected in the stratosphere (Brownlee 1 985). The class of chondritic porous IDPs are thought to be of cometary origin because of their unequilabrated mineral mixture, high carbon content, and relatively high atmospheric entry velocities. These

aggregate particles are typically composed of grains a few tenths of a micron in diameter.

Modern computing power offers the possibility to compute the scattering properties of non-spherical particles by a variety of techniques. Most authors who have studied the scattering by aggregate particles create aggregates composed of compact units, hereafter "monomers", that are small compared to visual wavelengths. Yet West (1 991) and Zerull et al. (1 993) have shown that monomer size strongly influences the scattering by an aggregate particle.

Consequently, we have constructed aggregate particles as clusters of monomers which are similar in size to the grains in chondritic aggregate IDPs. Since scattering properties also depend on particle shape, we have examined two very different shapes for our monomers, spheres and tetrahedra. In this paper, we present our results for the cross sections, temperature, phase function, and polarization of aggregate structures and compare them with the remote sensing observations of cometary dust.

2 Aggregates and the DDA Method

2.1 Aggregate model of cometary *dust*

Following our astrophysical arguments in the preceding section, we represent cometary dust particles as aggregates of monomers. Monomers in one aggregate are further assumed identical in size, shape and constituent material. We have chosen to study two groups of aggregates, namely, aggregates consisting of 4 monomers and of 10 monomers (Figure 1). In the former group, 3 monomers are positioned orthogonally with regard to the 4th monomer ("center"). In the later, one monomer is positioned at the center and the other nine are located around it more or less randomly. In each group, we further let the distances between surrounding monomers and the central one vary so that "Overlapping", "Touching" and " Separated" cases can be identified to roughly represent cometary dust particles with different porosities. The individual monomers may also take the shape of either a sphere or a tetrahedron. This will enable us to examine the possible shape effects of the constituent monomers. The choice of tetrahedron as one possible monomer shape is based on the considerations that such a shape renders the largest deviation from a convex regular shape like a sphere and tends to introduce more irregularity when monomers are packed together with random individual orientations in an aggregate.

The constituent particles in aggregate IDPs typically have dimensions a few tenths of a micron. Therefore, we have selected $r_m = 0.25\mu m$. At our reference wavelength of $0.6\mu m$ for the polarization calculations, this radius gives a size parameter $x_m = 2.62$, large enough to be well away from Rayleigh scattering. Some calculations were also performed

for $r_m = 0.50\mu m$. Here, we are limited by the memory size for storing the dipole array.

Figure 1

2.2 *The DDA Method*

The discrete dipole approximation (DDA) method is one of several discretization methods (Goedecke and O'Brien 1988, Draine 1988, Hage and Greenberg 1990) for solving scattering problems in the presence of a target with arbitrary geometry. It is a particular implementation of the method of moments (Harrington 1968) - a general prescription for discretizing the integral form of Maxwell's equations. Since Purcell and Pennypacker [1973] first applied it to astrophysical problems two decades ago, the DDA method has been improved greatly by researchers (Draine 1988, Goodman et al. 1991, Draine and Goodman 1993, Draine and Flatau 1994) and gained popularity among scientists due to its clarity in physics principle and a free implementation of it in FORTRAN (DDSCAT package, Draine and Flatau 1994). Basically the DDA method works by using a finite array of polarizable points to approximate the continuum target. These points thus acquire dipole moments in response to the local electric fields and interact with one another through their electric fields. It has the ability to compute the scattering properties of objects with arbitrary geometry if the necessary number of dipoles are used. The number of dipoles needed depends on the accuracy required. In principle, DDA can be arguably applied to an object of any type. In practice, its applicability is however limited by the capacity of computing resources and the nature of the problem. These issues will be further addressed

in the following paragraphs.

2.3 *Computational Consideration*

In our research work, we use the DDSCAT code (version 4b.1, Draine and Flatau 1994), developed by Draine and his collaborators, to calculate scattering properties of aggregates on supercomputers. In its original form, the DDSCAT code has been well tuned to run on workstations. When employing it on supercomputers, customization is necessary in order to utilize the advantages offered by the vector and parallel architectures of Cray machines. Generally, DDA calculations require choices of the locations and the polarizabilities of the dipole points which represent the objects. Auxiliary codes were thus developed to prepare the aggregate structures in our study as dipole arrays residing on a cubic lattice, which can be fed to the DDSCAT code as inputs. The Lattice Dispersion Relation (LDR) method is selected as the default to assign the dipole polarizabilities, because it has been shown to give the best numerical results (Draine and Flatau, 1994). We also modified the output format of the DDSCAT code so that the complex amplitude quantities are saved instead of the intensity as in its original form. In doing so, we gain the flexibility to obtain and study more types of scattering related quantities. This becomes especially helpful when dealing with the averaging over many particle orientations.

There are two criteria for validity of the DDA method: (1) the wave phase shift $\rho = |m|kd$ over the distance d between neighboring dipoles should be less than 1, (2) d must be small enough to describe the object shape satisfactorily. A detailed comparison study by Draine and Flatau [1994] demonstrated that scattering and absorption cross

sections can be calculated by the DDA method to accuracies of a few percent for objects with $|m| < 2$, provided that the criteria elaborated above are satisfied. Since the DDA method does not give preferential treatment to target geometry, their conclusion based on the examination of single and double compact spheres shall serve well as a guideline in the DDA related research work.

Our experience with the DDSCAT code further shows that a strict compliance with these criteria without regard to the resultant quantities may either lead to erroneous conclusions or waste of precious computing resources. For example, the Q efficiency factors are generally much less sensitive to those criteria, and it is usually sufficient to let the value of ρ be around 1 or possibly bigger. On the contrary, when dealing with the polarization problems, since the angular-dependent scattering amplitudes, especially in near backward directions, are small in magnitude and very sensitive to the fine structure of the aggregate, one should demand ρ to be around 0.5 or less.

We can estimate the typical number of dipoles needed to obtain a reliable computational result using the DDSCAT code. Take an individual spherical monomer in our aggregates as an example. When represented in 3-dimensional array of N_m dipoles, its volume is $N_m d^3$, which must be equal to $4\pi r_m^3/3$, where r_m is the monomer radius. This leads to

$$N_m = \frac{4\pi}{3}\left(\frac{r_m}{d}\right)^3 \tag{1}$$

Since d is related to ρ via $d = \rho/(|m|k)$ and wavenumber $k = 2\pi/\lambda$, one further has

$$N_m \approx 1040(\frac{r_m|m|}{\rho\lambda})^3 \qquad (2)$$

If one is interested in scattering properties at light wavelength $\lambda = 0.6\mu m$ and the material is chosen as highly absorbing glassy carbon for which $m = 1.88 + 0.71\ i$, N_m is estimated to be 611 for $\rho = 1$ at $r_m = 0.25/1?72$. Hence in this typical case, 600 dipoles per monomer are the minimum for computing the efficiency factors. A similar application of Eq. (2) for ρ = -0.5 gives 4885 dipoles per monomer as required for the polarization calculations.

'1'able 1 and 2

Listed in Tables 1 and 2 are a few parameters describing these two groups of aggregates. Cautions are needed when referring to the porosities listed here. Usually aggregates are described in terms of porosity, $P = 1 - V_p/V_s$ where V_p is the volume of the material in the aggregate and V_s is the volume of the sphere enclosing the aggregate. This concept makes sense when the material is fairly uniformly distributed within the volume enclosed by the sphere. In a very filamentary particle, where the material is not spread out uniformly within the cı1c1oscc1 volume, the concept breaks down. Light interaction occurs on a scale comparable to the wavelength and, if $x_m \geq 1$, the light interacts with the individual solid monomers. For our aggregate of 10 monomers, it is reasonable to define the total volume of the aggregate compared to that of a circumscribed sphere, and the above definition of porosity makes sense.

In the current study, we are primarily interested in the scattering properties of ag-

gregates randomly oriented in space. In its original form, the DDSCAT code allows for averaging over random orientations. However it is useful only when the computation of the! total average can be well fitted into a single batch queue on a supercomputer, which, in practice, always has an upper limit of CPU time to ensure the fairness among different users. As computation becomes CPU time intensive as in our study, it is not possible to have the total average completed within one single batch queue. There is a need to separate the calculation of scattering properties in single orientation and the averaging over many different orientations. We, thus, modified part of the DDA code and choose the output to be all four complex amplitudes of the scattering matrix. The average is further done by a few auxiliary codes. In doing so, we not only, in a way, overcome the restriction of lilnitcel-time batch queue, but also gain certain benefits of parallelism as offered in modern supercomputers. It is possible and advantageous to calculate scattering properties of several single orientations simultaneously, each of which is on a different processor. Given the multi-processor architecture of modern supercomputers, such an approach definitely improves the performance on either the speed or the size of the problem at hand.

Following the D D SCAT code's notation, a particle's spatial orientation is uniquely determined by three rotation angles: β, θ, ϕ. The polar angles θ and ϕ specify the direction of the particle's principal axis ill the Lab Frame. The object is then assumed to be rotated around this axis by an angle β. Our basic assumption in the current study is that aggregates in space are randomly oriented and scattering of light by each aggregate is independent of that of others. Following the practice of the authors of the DDSCAT code, we let the

sample points be distributed uniformly in the range of [0, 360) for both β and ϕ, and [--1, 1] for $cos(\theta)$. We use tuple $(n_\beta, n_\theta, n_\phi)$ to denote that there are n_β angles chosen for β, n_θ for θ and n_ϕ for ϕ.

3 Modelling Aggregates

3.1 The Cross sections

The wavelength dependence of the absorption cross section is the basic quantity for computing the temperature of small particles, whether cometary or interplanetary dust in the solar radiation field or dust in circumstellar disks. The absorption cross section is also necessary to relate the observed thermal flux to the mass of emitting dust.

Figure 2

1 Both IDPs and comet dust are carbon-rich and low in albedo. Thus, we used the wavelength-dependent refractive indices of glassy carbon from Edoh (1983) plotted in Figure 2. We have computed cross sections for 10-monomer aggregates at monomer size $r_m = 0.25\mu m$ and $0.5\mu m$. Presented in Figure 3 ($r_m = 0.25\mu m$) and Figure 4 ($r_m = 0.5\mu m$) are the wavelength dependent values of the cross sections (absorption, scattering and extinction) per volume, i. e., C_{abs}/V (μm^{-1}), C_{sca}/V (μm^{-1}), and C_{ext}/V (μm^{-1}) for aggregates in a single spatial orientation, assuming the light is coming from the bottom in Figure 1. The values for a single sphere and single tetrahedron of size equal to that of monomers in the aggregates are also plotted for comparison. The values for the single tetrahedron were also obtained using the DDSCAT code by averaging over (8,9, 32) spatial orientations. The single tetrahedron was represented by 673 dipoles at $\lambda \geq 3\mu m$ and 1 072G dipoles at $\lambda < 3\mu m$, to ensure $\rho = |m|kd \leq 1$ at both $r_m = 0.25\mu m$ and $r_m = 0.5\mu m$. The values for a single sphere were calculated by a standard Mie code. All computed values by

the DDSCAT code are represented as plus signs.

Figure 3 and 4

The asymptotic values of $C_{abs}/V, C_{sca}/V, C_{ext}/V$ for each aggregate as well as the single tetrahedron at $\lambda = 0$, were obtained by counting the number of dipoles in the volume and the number of dipoles projected onto the plane perpendicular to the incident light, and taking into account the fact that, at $\lambda = 0$, $Q_{abs} = 1$, $Q_{sca} = 1$ and $Q_{ext} = Q_{abs} + Q_{sca} = 2$. These values are used to extrapolate the values of cross sections for $\lambda \leq 1\mu m$.

For the aggregates shown in Figure 3 and 4, the validity criterion $\rho \leq 1$ is satisfied at $\lambda > 1\ \mu m$ os $2\mu m$ respectively. '] 'c? assure that the cross sections at $\lambda \leq 2\mu m$, including those by extrapolation at $\lambda \leq 1\mu m$, are accurate enough for our current discussion, wc have made onc more CPU-expensive calculation for the 10-monomer "Touching" aggregate of spherical monomers at $\lambda = 0.6\mu m$ and $r_m = 0.25\mu m$ using about 5100 dipoles per monomer. In this case, $\rho = |m|kd = 0.4934 < 1$. These results are plotted as triangles in Figure 3, and the relative differences arc smaller than 1% compared with the corresponding extrapolated values. This reflects the general insensitivity of Q efficiency factors to light wavelength at $x_m = 2\pi r_m/\lambda > 1$.

The filled circles in Figure 3 arc values calculated by averaging over (8,9, 32) spatial orientations for the 1 0-monomer "Touching" aggregate consi sting of tetrahedral monomers with $r_m = 0.25\mu m$ at $\lambda =]$, 2 and $20\mu m$. Their agreement with respective values for a single orientation confirms our general experience with the DDA method that cross

sections are not sensitive to the orientation for approximately equidimensional particles. Furthermore the geometric cross-section of our aggregates varies with orientation by < 2%. Thus we have confidence in using absorption values for a single orientation to model the temperature of cometary dust in the next section.

The cross sections shown in Figure 3 and 4 share a few general features, which are independent of monomer shape and size as wC]] as aggregate structure. All curves have a turn-over point around $x_{eff} = 1$, where x_{eff} is the volume-equivalent size parameter for aggregates and single tetrahedron. TIIc cross sections are almost flat for $x_{eff} > 1$, but exhibit various slopes at $x_{eff} < 1$. All C_{sca} /V *curves* follow λ^{-2} at longer wavelength as expected for Rayleigh scattering. Extinction cross sections resemble absorption cross sections closely since our aggregates are highly absorbing particles.

The C_{abs} /V *curve* for a single sphere varies as $\lambda^{-1.7}$ at long wavelength. The same slope holds for the "Separated" aggregate of spheres, for the light interacts primarily with the individual monomers. The "Overlapping" aggregate of spheres also resembles a single, but "effectively" larger sphere than its constituent monomer. However, the "Touching" aggregate produces a ICss steep Slope> $C_{abs} \sim \lambda^{-1}$. As for the aggregates consisting of tetrahedral monomers, the absorption also has a slope of $C_{abs} \sim \lambda^{-1}$. So does the absorption of a single tetrahedron. Consequently, at $\lambda \geq$ 100~/?n, the tetrahedral aggregates and the "Touching" spherical aggregate have C_{abs} values a factor of 5 or more higher than that Of a single sphere. This difference is important for relating submillimeter and mid-infrared observations and for estimating the mass of circumstellar disks from the submillimeter

fluxes. Our result is in agreement with that of Bazell and Dwck (1990), but in contrast to that of Kozasa *et* al (1 992). The latter didn't find an enhancement of the infrared flux for their aggregates compared to a sphere. Since their aggregates were very porous in structure, resembling more our "separated" aggregates of spheres, it is not surprising that the scattering properties arc similar to that of the constituent parti cles.

3.2 *The Equilibrium Temperature*

The equilibrium tempera.turcs of cometary dust aggregates arc calculated by equating the solar radiation absorbed to the thermal radiation emitted using the following equation:

$$\left(\frac{r_0}{r}\right)^2 = \left(\int_0^\infty 4\pi B(\lambda,T)C_{abs}(\lambda)d\lambda\right) \Big/ \left(\int_0^\infty S(\lambda)C_{abs}(\lambda)d\lambda\right) \qquad (3)$$

where r_0 =- 1 AU, r in AU is the heliocentric distance of the dust grain, $C_{abs}(\lambda)$ the absorption cross section of particles, $S(\lambda)$ the solar flux at 1 AU, and $B(\lambda,T)$ the Planck function for the emitting particle. The results calculated for 10-monomer aggregates arc shown in Figure 5.

Figure 5

It is evident from Figures 3 and 4 that aggregate structure, monomer shape, and size all influence the scattering prope rties. This result affects modeling the temperature properties of cometary dust. The temperatures in Figure 5 can be understood by reference to C_{abs}/V, specifically the ratio of C_{abs} at $\lambda < 1\mu m$, where the solar flux is absorbed, to C_{abs} at 1 - $20\mu m$, where the absorbed energy is reradiated. Hanner (1 983) showed

that absorbing spheres of radius less than 1.5pm will be hotter than a blackbody, with temperature inversely correlated with size, and we see that C_{abs} decreases steeply in the infrared for single spheres. Since the slope of C_{abs} in the infrared is less steep for the aggregates, we expect that aggregates of submicron monomers will tend to be cooler than a single monomer.

When the monomers are touching (porosity $P \approx 0.64$) or overlapping ($P \approx 0.3$), the temperatures are the same as those of a sphere with volume equivalent to the aggregate, within $\sim 3\%$. As the monomer separation increases, there is less interaction between them and the temperatures approach those of a single monomer. For the case of spherical monomers with $3r_m$ separation ("Separated" case $P \approx 0.84$), the temperatures are 4 — 6% lower than the monomer temperature. In contrast to the spheres, the "Separated" tetrahedra have temperatures significantly lower than a spherical monomer and about 5 - 8% lower than that of a single tetrahedral monomer. Thus, the transition between temperatures close to the monomer and temperatures close to the total volume equivalent sphere occurs at porosities > 0.64, regardless of monomer shape or size.

At small heliocentric distances, the Planck function peaks in the near-infrared, on the flat part of the C_{abs}/V curve, and thus the temperatures approach the blackbody temperature.

3.3 Degree of Polarization

The degree of polarization versus phase angle $\theta_p = 180^\circ - \theta$ (θ is the scattering angle) observed in comets is displayed in Figure 6. One sees negative polarization of a few percent

near the backscattering direction, a cross-over near $\theta_p = 20°$ and maximum polarization p_{max} near $\theta_p = 90°$. The negative branch and crossover point are remarkably consistent among comets, while p_{max} can vary between 0.10 - 0.25 (Levasseur-Regourd et al. 1996).

Figure 6

It is well known that polarization is strongly dependent on the shape, as well as the size and refractive indices of the scattering particle. In this section, we investigate how the aggregate structure and porosity influence the polarization and whether the polarization by small aggregates resembles that in comets, particularly the negative polarization at $\theta_p \leq 20°$.

'1'0 model the randomly oriented particles in the comet coma, it is necessary to have the scattering properties of our irregular aggregates averaged over all of the possible orientations, i.e., β : [0, 3600), θ : [0, 180°] and ϕ : [0, 3600). Since we have limited computing resources, it is necessary to know how many sample points are needed to achieve the desired accuracy. The answer to this strongly depends on the scattering properties under consideration as well as on the aggregate configuration.

In previous sections, it has been shown that the Q efficiency factors are not very sensitive to aggregate orientations, given that the aggregate has a more or less random structure. However, as we turn to the problem of polarization, the orientation dependence becomes complex and subtle. This is evident in Figure 7a, where the polarization curves are shown for a single tetrahedron with several spatial orientations. It is generally impossible

to predict the averaged behavior based on the polarization curve at individual orientations.

Figure 7a, b, c, d.

To investigate the necessary number of sample points for each of the three orientation angles, we choose a single tetrahedron because it renders strong irregularity when positioned arbitrarily in space. Following the practice of the authors of the DDSCAT code, we let the sample points to be distributed uniformly in the range of [0, 360°) for both β and ϕ and [- 1,]] for $cos(\theta)$. Tuple $(n_\beta, n_\theta, n_\phi)$ is used to demote that there are n_β angles chosen for β, no for θ and n_ϕ for ϕ. We let $m = 1.88 + 0.71i, \lambda = 0.6\mu m$ ant] the equivalent-volume radius $r_{eff} = 0.25\mu m$. The single tetrahedron is represented in an array of 10726 dipoles, which leads to $\rho = |m| kd = 0.3846$. Shown in Figure 7b are polarization curves of (1, 1, n_ϕ) with n_ϕ =- 4,8,16,32,64. Curves of (1, 1, 16), (1, 1,32) and (1, 1,64) are basically indistinguishable from each other. It is sufficient to set $n_\phi = 32$ from now on. Presented in Figure 7c are curves for (4, 5, 32), (8, 5, 32), (8, 9, 32), (16, 5, 32) and (16, 9, 32) and the differences between (16, 9, 32) and the rest are depicted in Figure 7d. It is evident that (8, 5, 32) already gives a good convergence around 1%. This kind of accuracy is sufficient for our current study. In our average calculation of aggregates, we use (16, 5, 32).

To find out how the polarization of aggregates depends on monomer/aggregate size, porosity, monomer shape, and, most important, when the "negative polarization" will appear, we carried out, computations for the two groups of aggregates as described in Section 2: aggregates consisting of 4 monomers and those of 1 O monomers (Figure 1). The

refractive indices used at $\lambda = 0.6\mu m$ is $m = 1.88 + 0.71i$ for glassy carbon, an absorbing material typical in cometary dust. Monomers of size $r_m = 0.25\mu m$ well represent the substructure in IDPs. The resultant polarization curves averaged over (16, 5, 32) spatial orientations are presented in Figure 8 and 9. Also plotted are polarization curves of corresponding Mic spheres with equivalent volume, which are on the right hand side. In each figure, polarization by a single sphere or tetrahedron of the monomer size is shown on top and bottom. These shall represent the asymptotic cases of '(fully overlapping" or "totally separated", which serve as good references when discussing porosity effects. The curves for the single tetrahedron are averaged over (1 G, 5, 32) too. It must be noted that we were not able to obtain the results for the "Separated" aggregates of 10 monomers, since the memory requirements for committing such calculations are beyond the capacity of the Cray machines we USC.

Figure 8 and Figure 9

Figures S and 9 show that both monomer size ant] shape and aggregate porosity influence the polari zation. Clearly, equivalent volume spheres are a poor approximation to the polarization by aggregates, even aggregates of spherical monomers. Thus, the old practice of using a volume-equivalent compact sphere to represent all aggregate is not reliable for polarization calculations.

Aggregate structure tends to mute the amplitude of features seen in the monomer polarization. This is true for both spheres and tetrahedra and is most evident in the

"Touching" case. For all 4 of our "'Touching" aggregates, the features are smoothed and the trend is toward a broad maximum of $p_{max} \sim 0.5$. The anticipated trend with porosity is evident if the curves at the left hand side of each figure arc observed; i.e., polarization by an aggregate will converge to that of a single compact monomer as the monomers in the aggregate become fully overlapping or widely separated. Our "Separated" case ($P = 0.84$) differs little from a single monomer.

Polarization curves can largely be understood when one tries to visualize aggregates in the "wavelength way". The light sees particles in scales measured by its wavelength. It will not be able to scrutinize st ructures much large.r or smaller that its wavelength. This is very w e l l reflected in the polarization curves. For "Overlapping" and "Touching" aggregates, the light sees more or less a compact particle with larger size. That is why more oscillatory features arc seen in the polarization curve. When coming into "Separated" aggregates, the light can not be fooled and sees the interspace between monomers, thus view the total aggregate as an ensemble of monomers.

If the monomers arc tetrahedra, the polarization curves of aggregates seem to be smoother than those of aggregates with spherical monomers. This is probably because aggregates consisting of tetrahedral monomers have more irregularity in structure. This kind of irregularity has a dimension in the range of the light wavelength and makes noticeable contributions to polarization, which lead to many, but tiny, oscillatory features. The net result of this is an apparently smooth polarization curve.

The number of monomers in aggregate comes into play via contributing material.

Larger number means more material in aggregate, thus, a bigger particle, resulting in feature-abundant polarization curve. One interesting thing to note is that, in Figure 9, the polarization curves of "Touching" aggregate show a relatively sharp feature around $\theta = 30$ for both of spherical and tetrahedral types. Wc firstly suspected that there might be a flaw in the DDSCAT code. After comparing them with corresponding ones of equivalent-volume Mic sphere, wc were much convinced that this is not artificial. This near-forward-direction feature seemly has something to do with the structure of aggregate rather than the shape of individual monomer.

Some calculations have been done for $r_m = 0.5\mu m$. The results for 4-monomer "Touching" aggregates are shown in Figure 10. Wc have used the same dipole arrays as in the calculation Of $r_m = 0.25\mu m$, which have already reached the upper limit of memory size on the Cray machines accessible to us. One concern here is whether the computational results at this monomer size can be trusted since the value of $\rho = |m|kd$ is now around 1. Hence one more calculation] was performed for the 1 0-spherical-monomer "Touching" aggregate at monomer size $r_m = 0.25\mu m$, using a dipole array with numbers halved in each spatial dimension ($\rho = 0.9861$). The polarization curve is plotted together with the one obtained by full size dipole array ($\rho = 0.4934$) in Figure 1 1. Both curves are spatial orientation averages over (1, 1, 64). They follow each other closely with a general deviation less than 0.05. 'Thus Wc are confident to use Figure 10 for $r_m = 0.5\mu m$ in our discussion of the general trends.

Figure 10 and Figure 11

By comparing Figure 10 with Figure. 8 of the same aggregate, we see stronger deviation cause by monomer shape at larger aggregate size. Following our argument in preceding paragraphs, the 4-tetrahedral-monomer aggregate of $r_m = 0.5\mu m$ seems to have larger irregularity as seen by light of $\lambda = 0.6\mu m$ than that of $r_m = 0.25\mu m$. Since the scale of wavelength and particle size are mutual translatable, we suggest that irregularity is likely wavelength dependent.

Clearly, none of the above curves for absorbing aggregates exhibits negative polarization near the backscatter direction like the comet dust does. Since dielectric material like silicate is able to produce larger negative polarization, we also computed cases for silicate material with In =] .65 -| 0.01i. Shown in Figure 12 are the polarization curves for the 4-spherical-monomer and 10- tetrahedral-lnonomer "Touching" aggregates with $r_m = 0.25\mu m$.

Figure 12

The 10-tetrahedral-monomer silicate aggregate begins to resemble the comet dust polarization, with small positive polarization over much of the range and negative polarization at phase angles < 40° . The polarization of the aggregate is quite different from that of an equivalent volume sphere, which exhibits strong resonances and large negative polarization. It is qualitatively similar to the small degree of polarization measured by

Giese et al. (1978) for a fluffy particle with $m = 1.5$, size parameter ≈ 20. Comparing the absorbing and silicate aggregates, one sees that there is plenty of space to create a polarization curve more closely resembling the comet polarization by mixing carbonaceous and silicate material.

Shown in Figure 13 is an example for the 10-tetrahedral-monomer "Touching" aggregate with $r_m = 0.25\mu m$. The ratio of carbonaceous to silicate aggregates is 5.75, in order to give roughly equal contributions to the scattered light, and we have computed the weighted average. Clearly, this mixture gives reasonable fits to both the negative polarization of a few percent near the backscatter direction and moderate positive polarization peaked around $\theta_p = 90°$. Our result is consistent with the evidence from IDPs and from the Halley dust composition analyzer (Kissel et al 1986) that comet dust is a mixture of both carbonaceous and silicate material.

Figure 13

3.4 Phase Function

Phase functions of our two groups of aggregates are displayed in Figure 14. Computational parameters are the same as those in the preceding section, namely, monomer size $r_m = 0.25\mu m$ and $m = 1.88 + 0.71i$ at $\lambda = 0.6\mu m$. We have followed the definition of phase function in Bohren and Huffman (1983) as $p = \frac{1}{C_{sca}} \frac{dC_{sca}}{d\Omega}$, where the differential scattering cross section $\frac{dC_{sca}}{d\Omega} = \frac{S_{11}}{k^2}$ and S_{11} is the first element of the scattering matirx.

Figure 14

Clearly phase functions exhibit less variations with regard to aggregate structure, size and monomer shape. Structure in the phase function at intermediate scattering angles, characteristic of the scattering by single spheres, is smoothed out for the aggregates. For aggregates of the same spatial structure but different monomer shape, their phase functions are very similar. The width of the forward scattering lobe is related to the total cross section of the aggregate, rather than to the size of the monomers, i.e., 10-monomer aggregates have narrower but stronger lobes than 4-monomer aggregates having the same size monomers and the forward scattering lobe is broader for the overlapping aggregates than for the "Touching" or "Separated" aggregates. For the "Touching" and "Separated" aggregates, an equivalent-volume sphere does not match the forward scattering; an equivalent area sphere would be a better approximation (e.g. West 1991).

For the aggregates of absorbing material as above, we find very little increase in the phase function near the backscattering direction; the ratio $I(180°)/I(150°)$ is, at most, 1.2. This contrasts with the comet phase function, where the rise from 150° to 180° is about a factor of 2 (Minis et al. 1982). It also contrasts with the laboratory measurements of the scattering by somewhat larger absorbing aggregates, size parameter 20 - 30 (Hanner et al. 1981; Giese et al. 1978), which exhibit a backscattering rise of a factor ~ 1.7.

Silicate spheres show a strong backscatter rise. Yet, the measured phase functions for aggregates with $m = 1.5$ and $x \approx 20$ are flat (Giese et al, 1978; Hanner et al. 1981). Figure

1 5 presents our comp uted phase functions for "Touching" aggregates of 10 tetrahedral silicate monomers, $m = 1.65 + 0.01i$ and $r_m = 0.25\mu m$. The ratio $1(180°)/1(1500)$ is 1.4, larger than that of absorbing aggregates.

Figure 15

Figure 16 is the phase function for the mixture of carbon and silicate aggregates as in Figure 13. It also shows a rise near the backward direction. The ratio $1(180°)/1(1500)$ is around 1.4 too. Thus, this mixture can give an approximate match to both the polarization and phase function at large θ for the comet ary dust.

Figure 16

4 Conclusions

In this paper, we have investigated scattering properties of aggregates, emphasizing the size of constituent monomers comparable with the wavelength of visible light. This has differentiated our study from previous investigations of aggregates in which the size of the monomers was much smaller than the wavelength. Our main motivation has been to model the scattering properties of cometary dust analogs. Cometary dust particles are expected to be aggregates of compact grains a few tenths of a micron in diameter, based on the structure of chondritic aggregate IDPs. Our results are also relevant to other astrophysical environments in which grain growth by aggregation has occurred, such as accretion disks surrounding young stellar objects.

Absorption cross sections of the aggregates tend to have less steep slopes towards longer wavelength, $C_{abs} \sim \lambda^{-1}$. The steepness, however, is influenced by aggregate structure and monomer shape. "Touching" aggregates (Porosity $\approx$ 0.6) appear to deviate the most from equivalent volume spheres. An irregular monomer shape like a tetrahedron also makes the slopes of the aggregates much flatter. This leads to an enhancement of absorption at $\lambda \geq$ 100~17n, which has a direct implication on estimating the mass of circumstellar disks from the observed submillimeter flux.

The difference in the absorption by aggregates from that of compact spheres also affects modelling the equilibrium temperature of cometary dust in the solar radiation field. Aggregates of carbonaceous material are cooler than the individual monomers, because the aggregates radiate more efficiently in the infrared. But, when the porosity is high, ($\sim$ 0.8

or higher) the temperature will be close to the monomer temperature. These results are also applicable to determining the temperature versus distance from the central star in accretion disks or debris disks such as β Pictoris.

Cometary dust produces negative polarization of a few percent near the backscatter direction. We have searched for negative polarization near the backward direction for a range of aggregate size and structure, taking care to average over a large number of orientations to make the modelling results reliable. It is evident from our computational results that the old practice of using volume-equivalent spheres to represent the polarization by aggregates is misleading and, most of the time, erroneous. The polarization is sensitive to the shape and size of the constituent monomers as well as to the fine structure of the aggregate.

Generally, aggregates of highly absorbing material produce strong positive polarization around $\theta_p = 90°$, but no negative polarization near the backward direction. On the contrary, silicate aggregates are the major source of strong negative polarization at larger scattering angles. We have been able to mix the aggregates of both carbon and silicate and the resultant polarization curve (Figure 13) largely resembles the observation for comets (Figure 6), especially the negative polarization at $\theta_p \leq 20°$ and the maximum peak around $\theta_p = 90°$. The same mixture of carbonaceous and silicate aggregates also gives a reasonable rise of the phase function near the backward direction, which is consistent with both observation and experiment.

Thus, we find that aggregates with constituent monomers a few tenths of a micron in

size and with intermediate porosity ($\approx$ 0.6), as represented by our "Touching" aggregates, are a reasonable analog for cometary dust. That is, the chondritic aggregate IDPs thought to originate from comets are generally consistent with the observed scattering properties of cometary dust.

Acknowledgements

This research was supported at the Jet Propulsion Laboratory, California Institute of Technology, under contract with the National Aeronautics and Space Administration (Planetary Atmospheres Program). The Cray supercomputers used in this investigation were provided by funding from NASA offices of Mission to Planetary Earth, Aeronautics, and Space Science. The DDSCAT numerical code (version 4b) was obtained from `ftp://astro.princeton.edu/draine/scat/ddscat/ver4b`. Z. Xing was supported *by* a National Research Council Postdoctoral Fellowship.

References

Bazell, D., Dwek, E., 1990, Ap J 360, 142

Bohren, C. F., Huffman, D.R., 1993, Absorption and Scattering of Light by Small Particles, John Wiley & Sons, New York

Browlee, D. E., 1985, Ann. Rev. Earth Planet. Sci. 13, 147

Draine, B. T., 1988, ApJ 333, 848

Draine, B.T., Goodman, J. J., 1993, ApJ 405, 685

Draine, B.T., Flatau, P.J., 1994, J. Opt. Soc. Am. A 11, 1491

Edoh, O. 1983, Ph.D. dissertation, Dept. of Phys., Univ. of Arizona

Giese, R.H., Weiss, K., Zerull, R. H., Ono, T. 1978, A & A 65, 265

Goedecke, G.H., O'Brien, S. G., 1988, Appl. Optics 27, 2431

Goodman, J. J., Draine, B.T., Flatau, P. J., 1991, Optics Letters 16, 1198

Hage, J. I., Greenberg, J. M., 1990, ApJ 361, 251

Hanner, M. S., Giese, R.H. I., Weiss, K., Zerull, R., 1981, A & A 104, 42

Hanner, M. S., 1983, in Cometary Exploration, ed. T.I. Gombosi, Vol 2, p.1

Harrington, R.F., 1968, Field Computation by Moment Methods, Macmillan, New York

Kissel, J. et al, 1986, Nature 321, 280 and 336.

Kozasa, T., Blum, J., Mukai, T., 1992, A & A *263, 423*

Kozasa, *T., 13111111,* J., Okamoto, H., Mukai, q'., 1993, A & A 276, 278

Levasseur-Regourd, A .C., Hadamcik, E., Renard, J.B., 1996, A & A, in press

Meakin, P., Donn, B., 1988, ApJ 329, 1,39

Minis, R. L., A'Hearn, M. F. and Thompson, D.T., 1982, AJ 87, 1310

Praburam, G., Goree, J., 1995, ApJ 441, 830

Purcell, E.M., Pennypacker, C. R., 1973, ApJ 186, 705

West, R. A., 1991, Appl. Optics 30, 5316

Zerull, R. H., Gustafson, R. A. S., Schulz, K., Thiele-Corbach, E., 1993, Appl. Optics 32, 4088

Figure Captions

Fig. 1. 1 0-monomer aggregates represented in dipole arrays.

Fig. 2. Wavelength-dependent refractive indices for glassy carbon (Edoh 1983).

Fig. 3. Cross sections per volume versus wavelength for 10-monomer aggregates of glassy carbon. $r_m = 0.25$ p m. (a) C_{abs}/V, (b) C_{sca}/V, (c) C_{ext}/V. For detailed description of various symbols, please see the text. The curves for aggregates of tetrahedral monomers and a single tetrahedron have been shifted by a factor of 100.

Fig. 4. *Cross* sections per volume versus wavelength for 1 0-monomer aggregates of glassy carbon. $r_m = 0.5\mu m$. (a) C_{abs}/V, (b) C_{sca}/V, (c) C_{ext}/V.

Fig. 5. Equilibrium temperature modelled for 10-monomer aggregates. (a) $r_m = 0.25\mu m$, spherical monomer; (b) $r_m = 0.25\mu m$, tetrahedral monomer; (c) $r_m = 0.5\mu m$, spherical I1IO11OI11C1; (d) $r_m = 0.5\}\ \mu m$, tetrahedral monomer. Short dashed line: Overlapping, Long dashed line: Touching) Dash-clot line: Separated, Thin solid line: Single sphere, Thick solid line: Single tetrahedron, Thin solid line with "BB": Blackbody.

Fig. G. Observed degree of polarization] in comets. Levasseur-Regourd et al. 1 996

Fig. 7. Degree of polarization for a single tetrahedron. $m = 1.88 - 0.71\ i$, $r_{eff} = 0.25\mu m$ (a) at a few orientations selected randomly; (b) averaged over only ϕ angle; (c) averaged over β, θ and ϕ angles (d) difference between (16, 9, 32) orientations and the other averages.

Fig. 8. Degree of polarization for 4-monomer aggregates compared with that of sill-gle monomer and equivalent-volume spheres. Monomer size $r_m = 0.25\mu m$. Left column:

curves for aggregates and single monomer; Right column: curves for equivalent-volume spheres, numbers labeled are equivalent-volume radii. (a) spherical monomers; (b) tetrahedral monomers.

Fig. 9. Similar to Figure 8, but for 10-monomer aggregates. Monomer size $r_m = 0.25\mu m$. (a) spherical monomers; (b) tetrahedral monomers.

Fig. 10. Degree of polarization for 4-monomer "Touching" aggregates compared with that of equivalent-volume sphere. Monomer size $r_m = 0.5\mu m$. (a) spherical monomer; (b) tetrahedral monomer.

Fig. 11. Comprison between degrees of polarization calculated for different $\rho = |m|kd$ values for 10-spherical-monomer "Touching" aggregate. $m = 1.88 + 0.71i$, $\lambda = 0.6\mu m$ and $r_m = 0.25\mu m$.

Fig. 12. Degree of polarization for silicate "Touching" aggregates and all equivalent volume sphere. Monomer size $r_m = 0.25\mu m$, $m = 1.65 + 0.01i$ and $\lambda = 0.6\mu m$. (a) 4-spherical-monomer aggregate; (b) 10 tetrahedral monomers.

Fig. 13. Degree of polarization averaged for silicate and carbonaceous 10-tetrahedral-monomer "Touching" aggregates. Carbon: Silicate = 5.75.

Fig. 14. Phase function for 4-monomer and 10-monomer aggregates. $r_m = 0.25\mu m$, $m = 1.88 + 0.71i$. Solid line: spherical monomers; dotted line: tetrahedral monomers; dashed lines: equivalent-volume sphere.

Fig. 15. Phase function for silicate 10-tetrahedral-monomer aggregate. $r_m = 0.25\mu m$, $m = 1.65 + 0.01i$

Fig. 16. Phase function for a mixture of silicate and carbonaceous 10-tetrallcdxal-1I1OI1O1I1CI aggregate. $r_m = 0.25/1771$.

Table 1 Parameters of Aggregates for Cross Section Calculation

Aggregates of 10 spherical monomers

Aggregate	D/r_m	N_a	N_m	N_E	P	r_{eff}
Overlapping	1	3936	672	5616	0.30	0.9013
Touching	2	6361	636	17256	0.63	1.0077
Separated	3	6957	696	33552	0.79	1.0077

Aggregates of 10 tetrahedral monomers

Aggregate	D/r_m	N_a	N_m	N_E	P	r_{eff}
Overlapping	1	4179	744	8144	0.49	0.8888
Touching	2	6395	645	20672	0.69	1.0077
Separated	3	6413	641	44720	0.s6	1.0077

D: Center-center distance between the surrounding monomer and the central one.
r_m: equivalent-volume radius of monomer.
N_a: Number of dipoles in aggregate
N_m: Number of dipoles per monomer
N_E: Number of dipoles in a big imaginary sphere enclosing aggregate
P: Porosity defined as $1-N_a/N_E$
r_{eff}: Equivalent-volume radius of aggregate with $r_m = 0.5\mu m$

Table 2 Parameters of Aggregates for Degree of Polarization Calculation

$\lambda = 0.6\mu m, m = 1.88 + 0.71i$

$r_m = 0.25\mu m, x_m = kr_m = 2.61799$

4 Spherical Monomers

Aggregate	D/r_m	N_a	Extent(Extended)	r_{eff}	x_{eff}	ρ
Overlapping	1.0	15514	35 × 35 × 30 (36 × 36 × 30)	0.3592	3.76111	0.4885
Touching	2.0	20287	48 × 50 × 38 (48 × 50 × 40)	0.3969	4.15581	0.4936
Separated	3.0	20095	61 × 63 × 46 (64 × 64 × 48)	0.3969	4.15581	0.4952

4 Tetrahedrall Monomers

Aggregate	D/r_m	N_a	Extent(Extended)	r_{eff}	x_{eff}	ρ
Overlapping	1.0	15536	49X46X44 (50X48X45)	0.3592	3.76111	0.4883
Touching	2.0	21016	64x60x52 (64x60x54)	0.3969	4.15581	0.4878
Separated	3.0	20883	76X74X61 (80X75X64)	0.3963	4.15581	0.4952

10 Spherical Monomers

Aggregate	D/r_m	N_a	Extent(Extended)	r_{eff}	x_{eff}	ρ
Overlapping	1.0	31456	41X41X40 (45x45x45)	0.4440	4.65375	0.4776
Touching	2.0	50786	58x59x62 (60x60x64)	0.5386	5.64030	0.4934

10 Tetrahedral Monomers

Aggregate	D/r_m	N_a	Extent(Extended)	r_{eff}	x_{eff}	ρ
Overlapping	1.0	29215	57 × 46 × 56 (60 × 48 × 60)	0.4440	4.65375	0.4776
Touching	2.0	48867	74 × 62 × 74 (75 × 64 × 75)	0.5386	5.64030	0.4998

D: Center-center distance between the surrounding monomer and the central one

r_m: Equivalent-volume radius of monomer

N_a: Number of dipoles in aggregate

Extent: Extent of aggregate in 3-dimensional space

Extended: Extent of latitce required by the DDA code

r_{eff}: Equivalent-volume radius of aggregate

$x_{eff} = 2\pi r_{eff}/\lambda$

$\rho = |m|kd$

d: dipole spacing

Overlapping
Touching
Separating

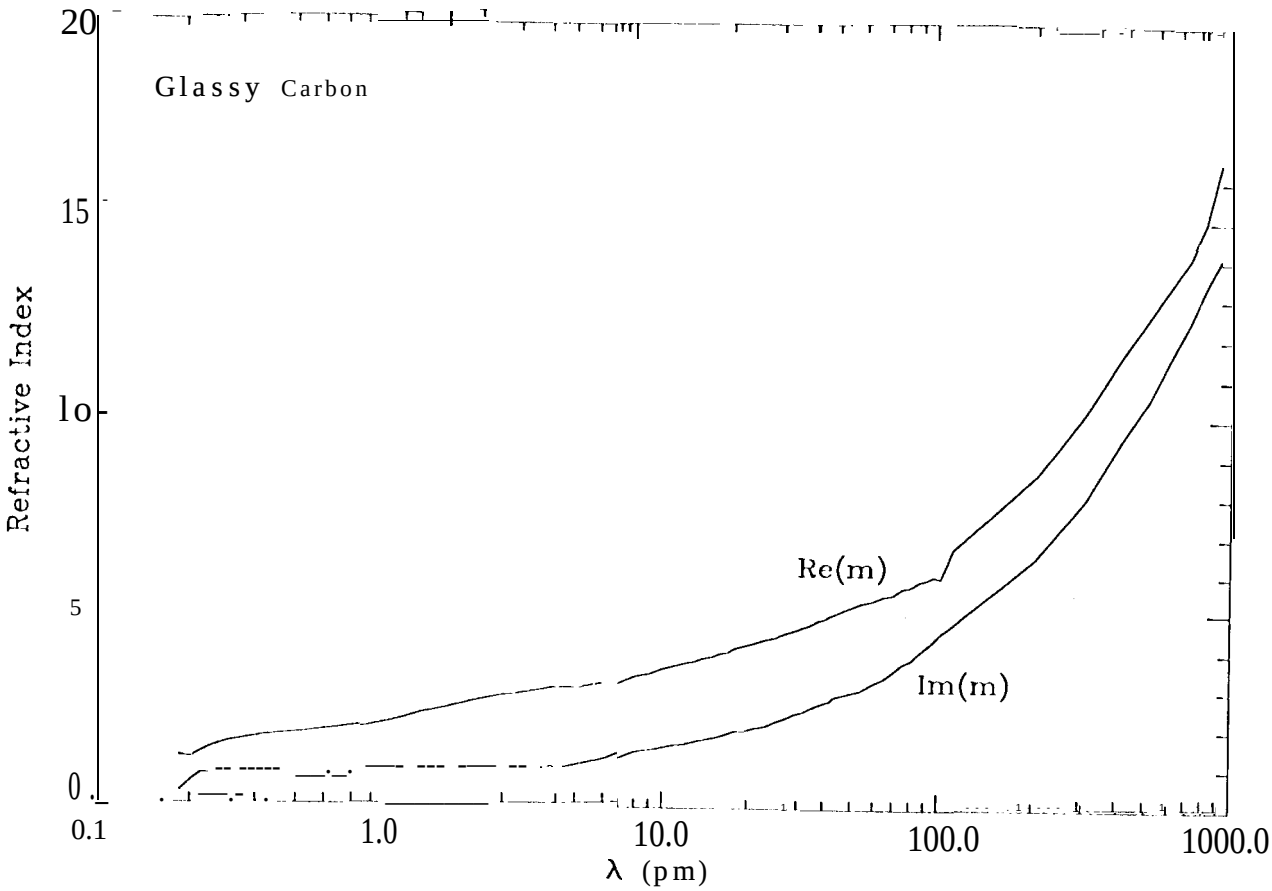
Glassy Carbon
Refractive Index
20
15
10
5
0
0.1
1.0
10.0
100.0
1000.0
λ (pm)
Re(m)
Im(m)

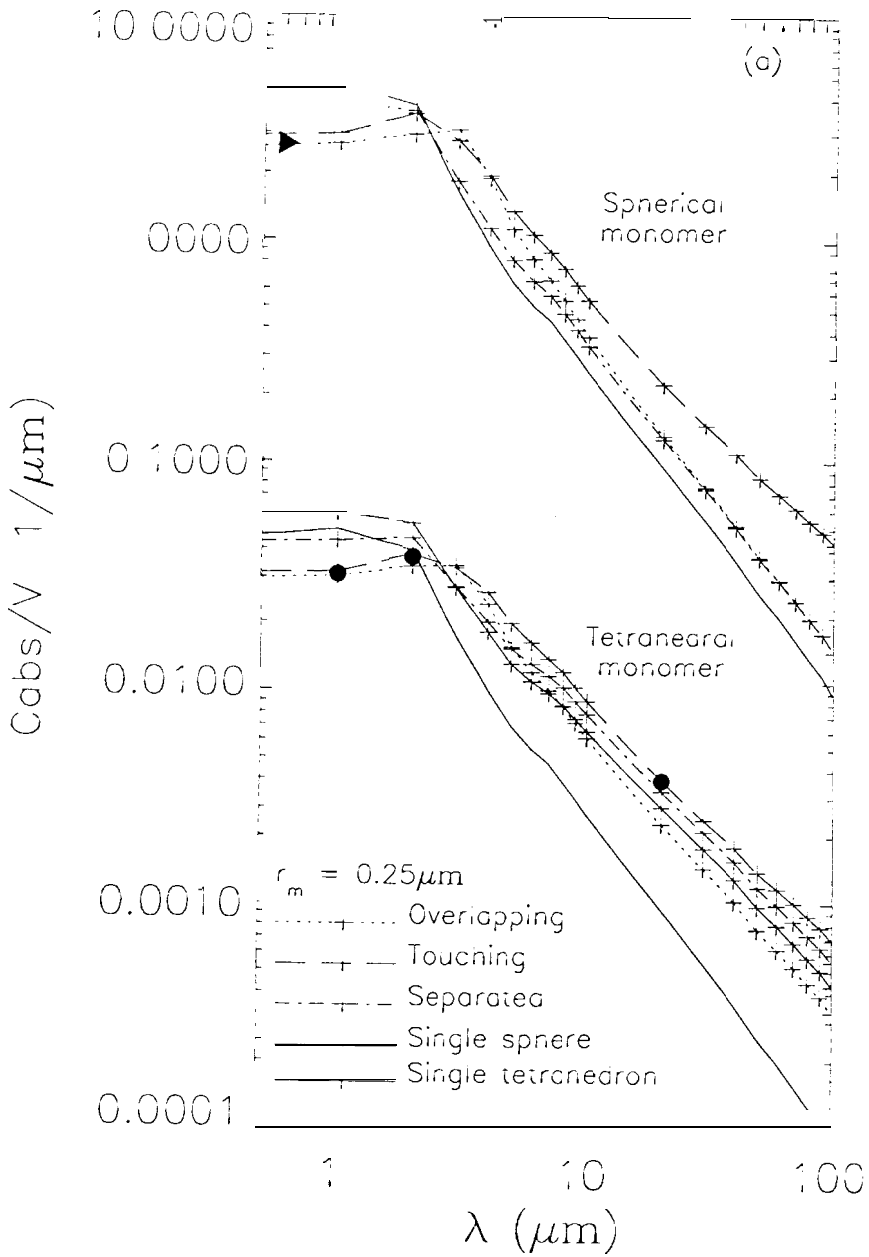
10 0000
0000
0 1000
0.0100
0.0010
0.0001
Cabs/V 1/(μm)
(a)
Spherical monomer
Tetrahedral monomer
r_m = 0.25μm
Overlapping
Touching
Separated
Single sphere
Single tetrahedron
1
10
100
λ (μm)

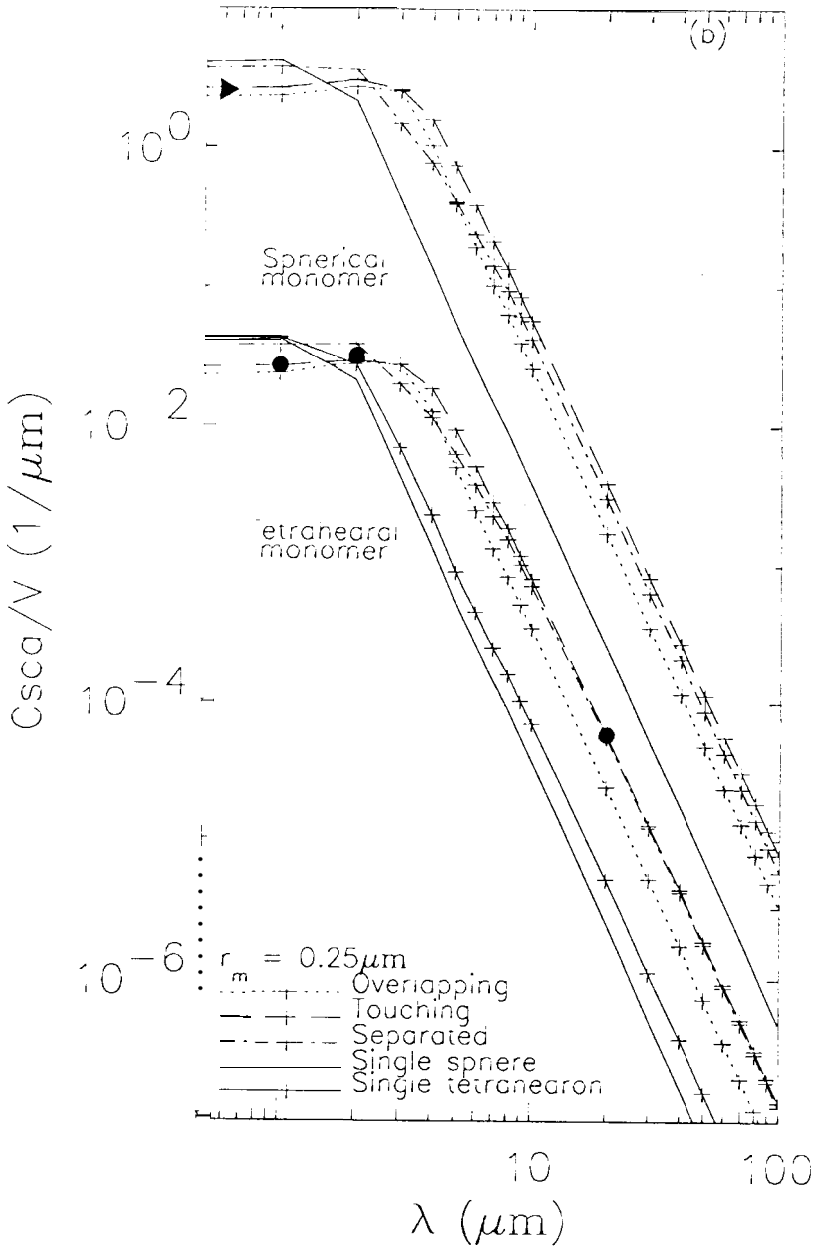
(b)
Spherical monomer
Tetrahedral monomer
r_m = 0.25μm
Overlapping
Touching
Separated
Single sphere
Single tetrahedron
Csca/V (1/μm)
λ (μm)
10^0
10^{-2}
10^{-4}
10^{-6}
10
100

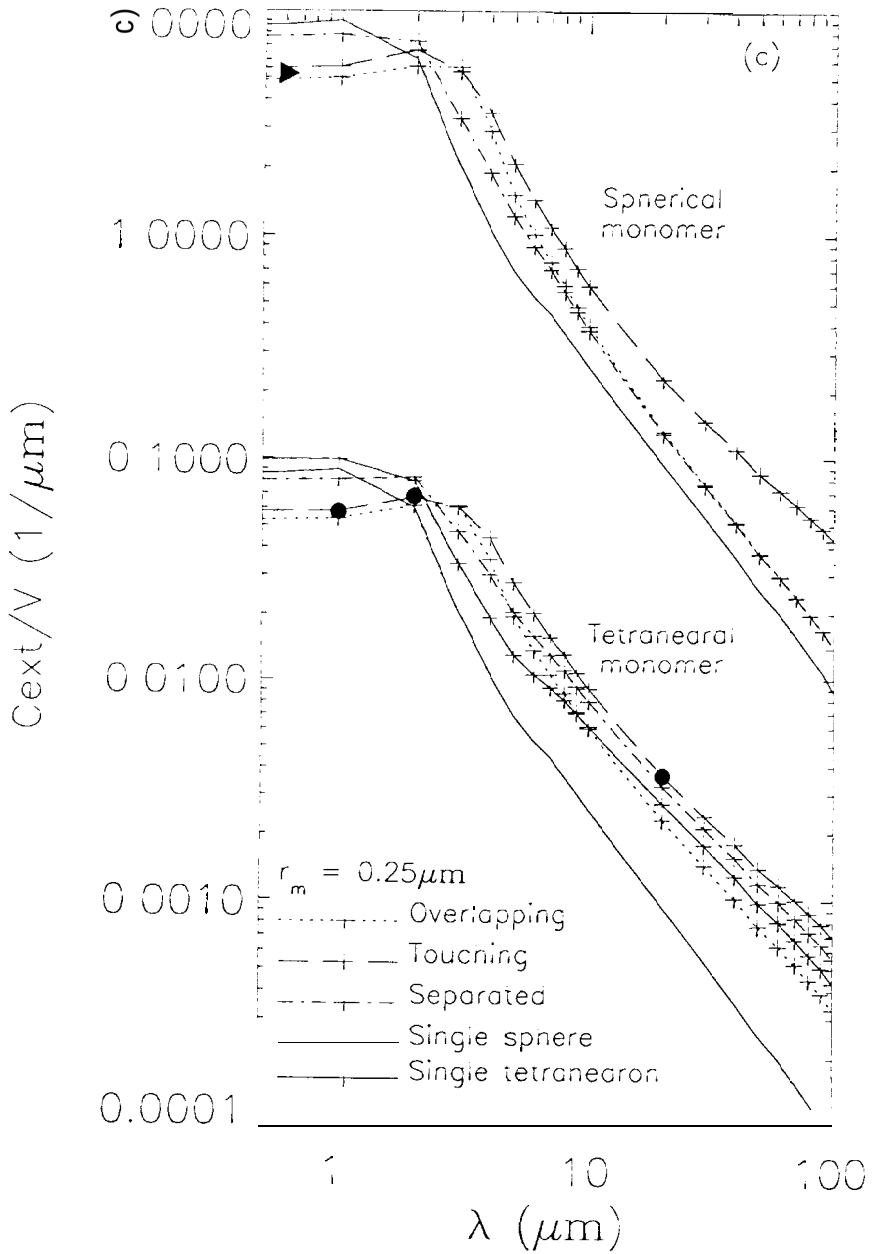
c) 0000
1 0000
0 1000
0 0100
0 0010
0.0001
Cext/V (1/μm)
(c)
Spherical monomer
Tetrahedral monomer
r_m = 0.25μm
Overlapping
Touching
Separated
Single sphere
Single tetrahedron
1
10
100
λ (μm)

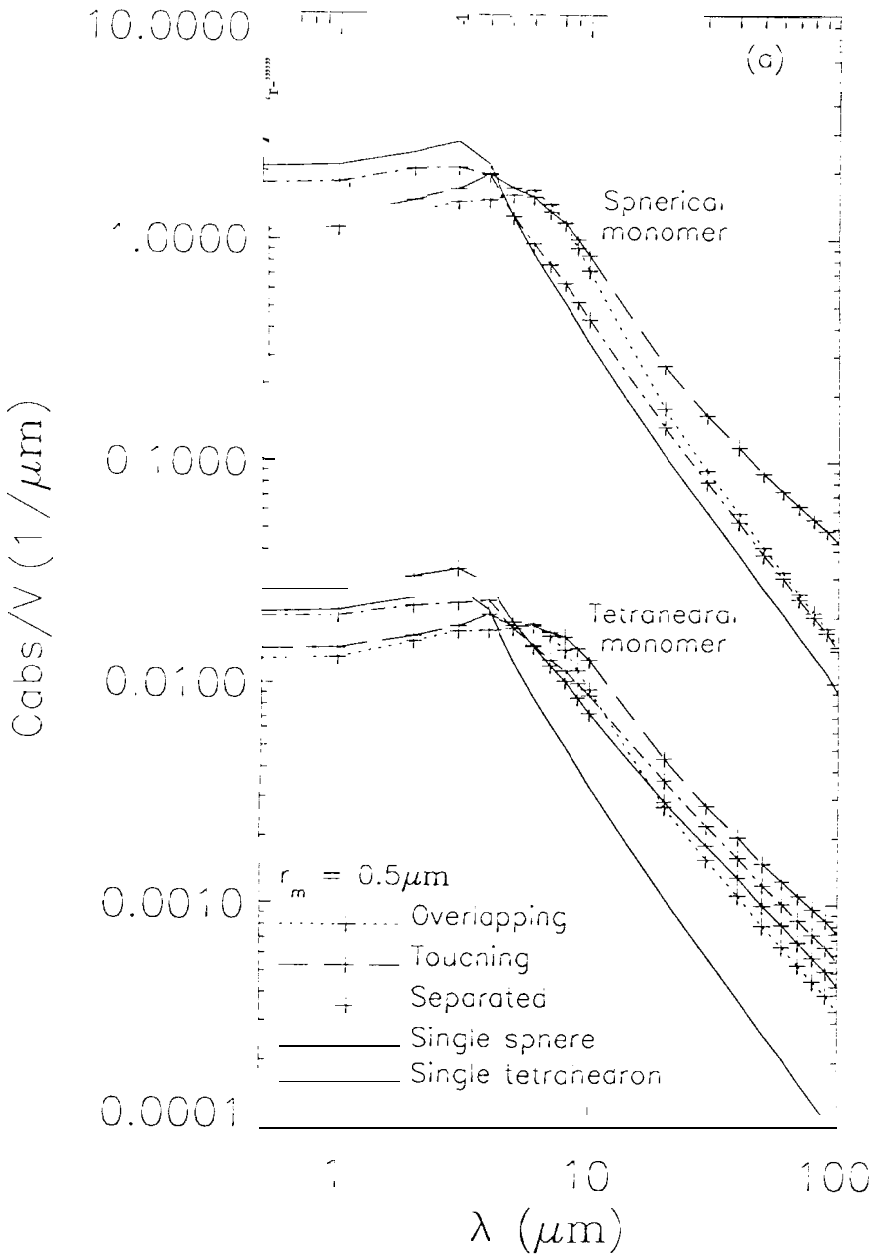
10.0000
1.0000
0.1000
0.0100
0.0010
0.0001
(a)
Spherical monomer
Tetrahedral monomer
r_m = 0.5μm
Overlapping
Touching
Separated
Single sphere
Single tetrahedron
Cabs/V (1/μm)
1
10
100
λ (μm)

Csca/V (1/μm)
λ (μm)
Tetrahedral monomer
Spherical monomer
r_m = 0.5μm
Overlapping
Touching
Separated
Single sphere
Single tetrahedron
(a)

Cext/V (1/μm)
10.0000
1.0000
0.1000
0.0100
0.0010
0.000
λ (μm)
1.00
1.0
(c)
Spherical monomer
Tetrahedral monomer
r_m = 0.5μm
Overlapping
Touching
Separated
Single sphere
Single tetrahedron

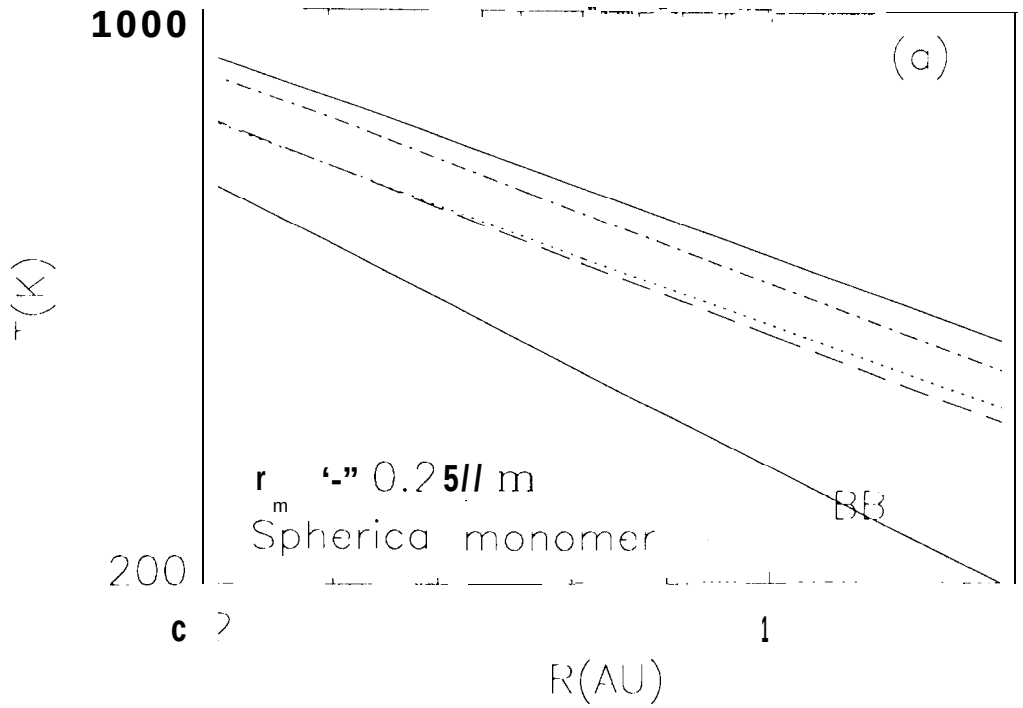

Fig. 5(a)

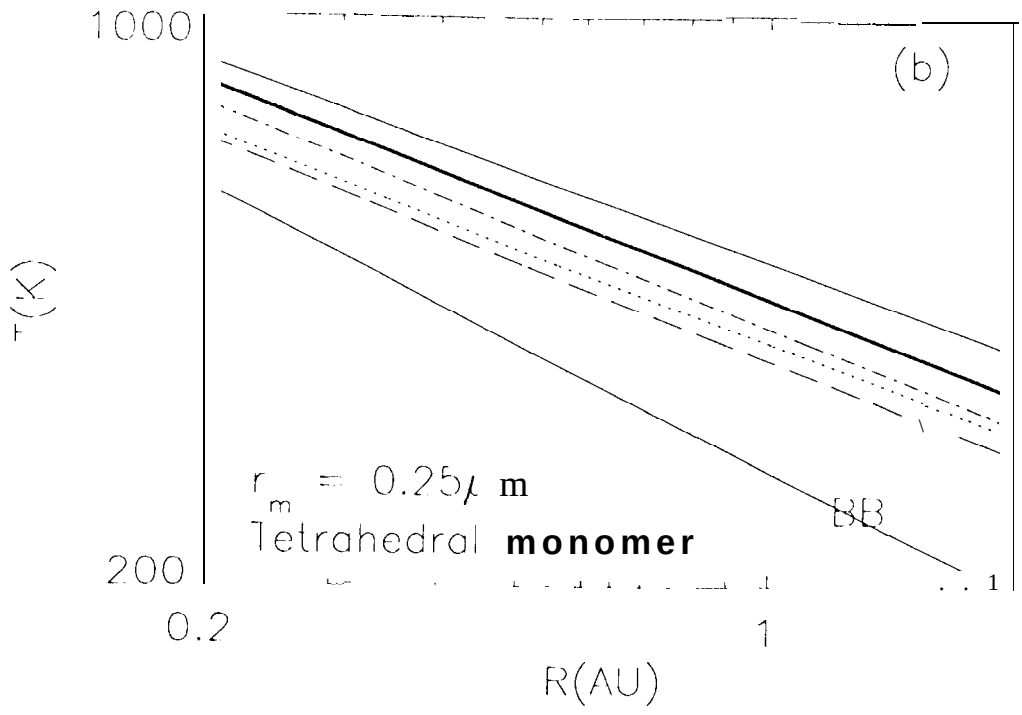
1000
200
0.2
1
R(AU)
T(K)
(b)
r_m = 0.25μ m
Tetrahedral monomer
BB

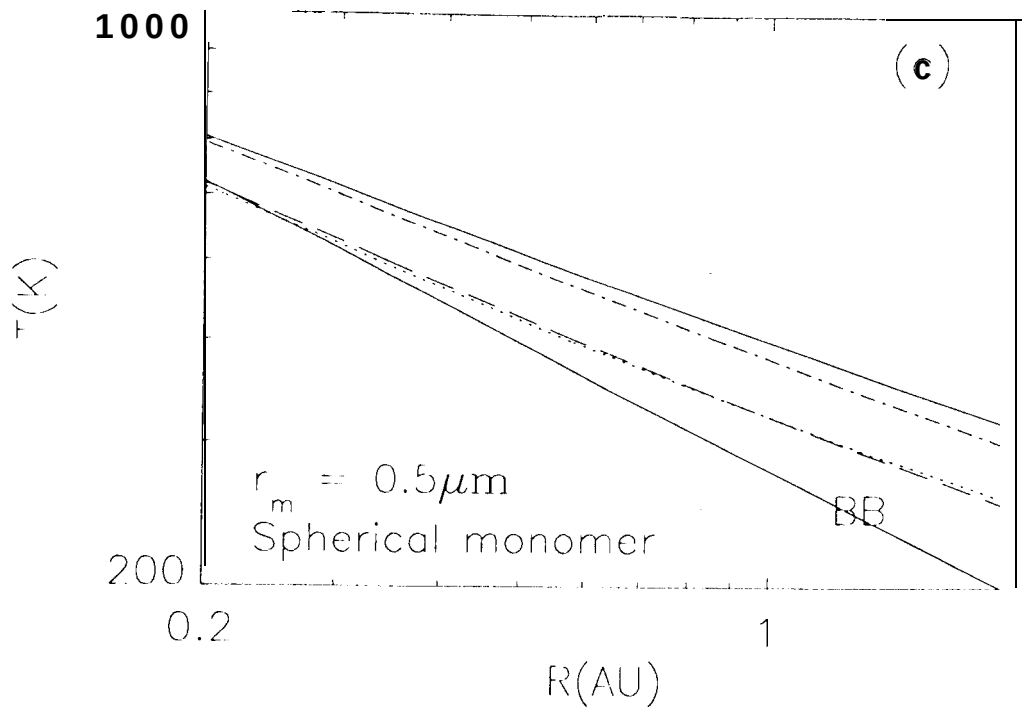
1000
(c)
T(K)
r_m = 0.5μm
Spherical monomer
BB
200
0.2
1
R(AU)

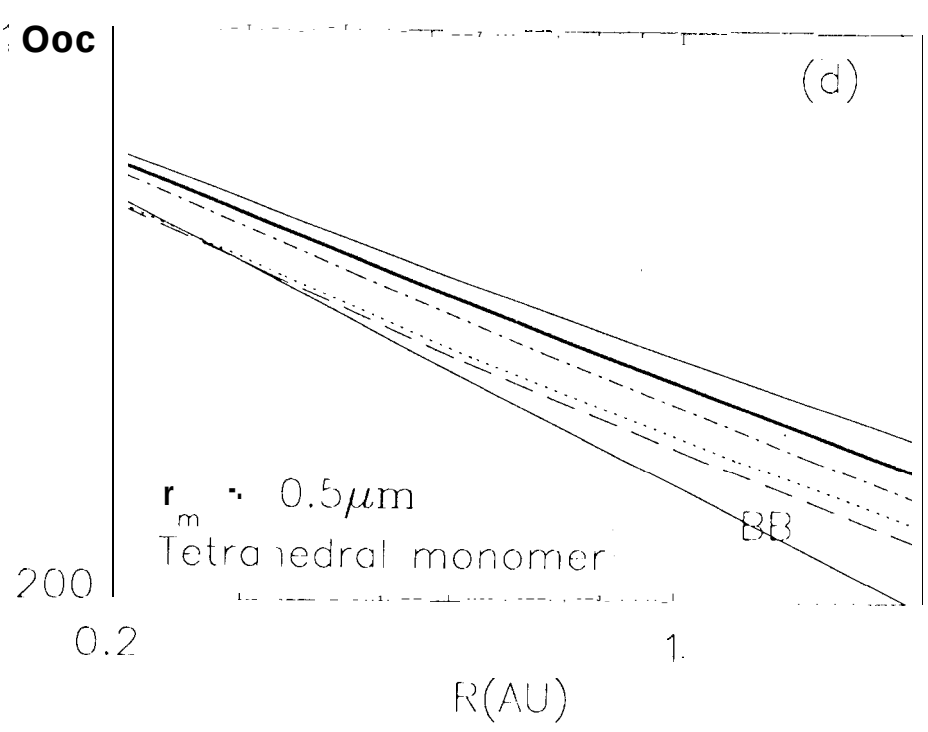

Fig. 5.10)

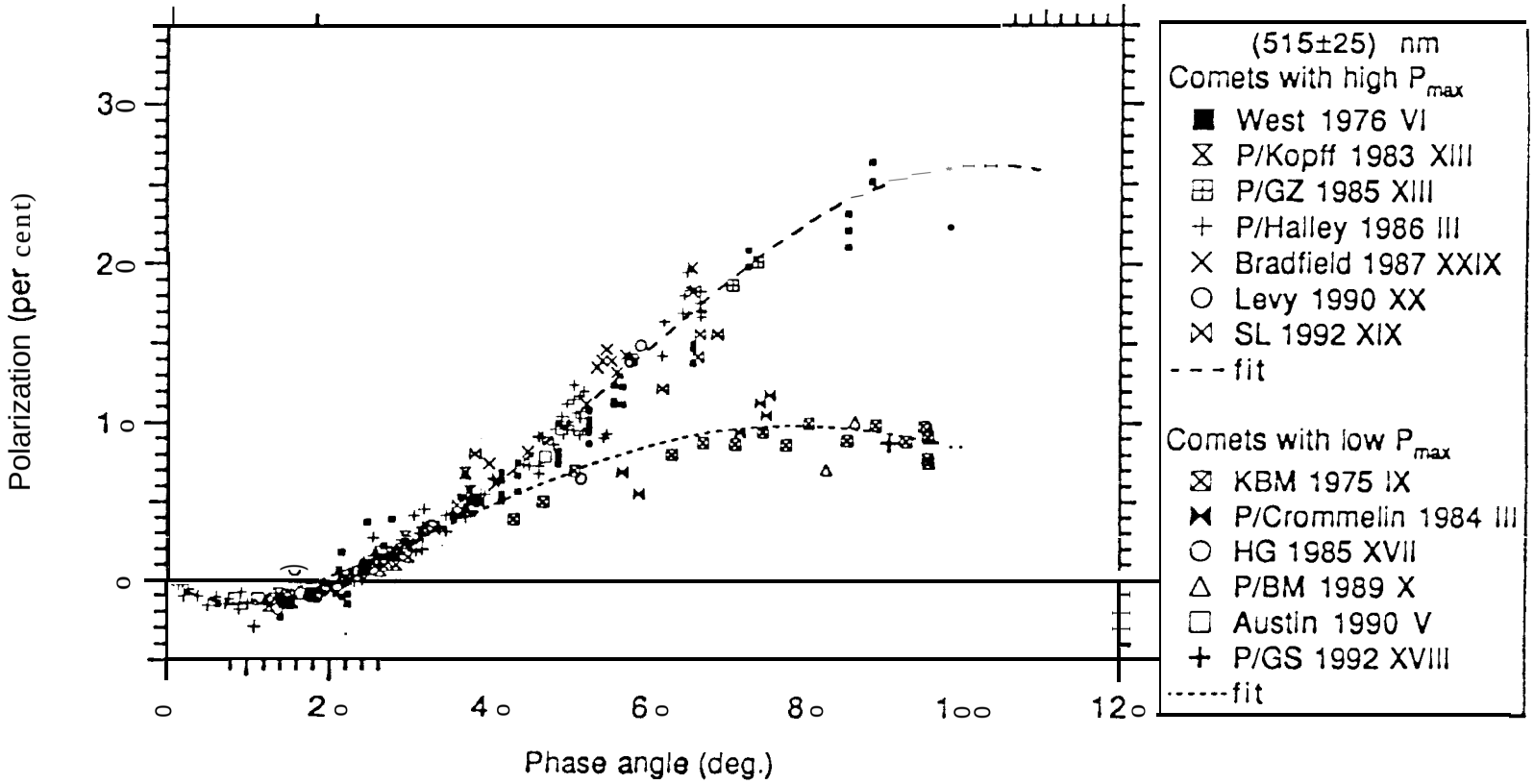
Polarization (per cent)
3o
2o
1o
o
o
2o
4o
6o
8o
1oo
12o
Phase angle (deg.)
(515±25) nm
Comets with high P_{max}
West 1976 VI
P/Kopff 1983 XIII
P/GZ 1985 XIII
P/Halley 1986 III
Bradfield 1987 XXIX
Levy 1990 XX
SL 1992 XIX
- - - fit
Comets with low P_{max}
KBM 1975 IX
P/Crommelin 1984 III
HG 1985 XVII
P/BM 1989 X
Austin 1990 V
P/GS 1992 XVIII
----- fit

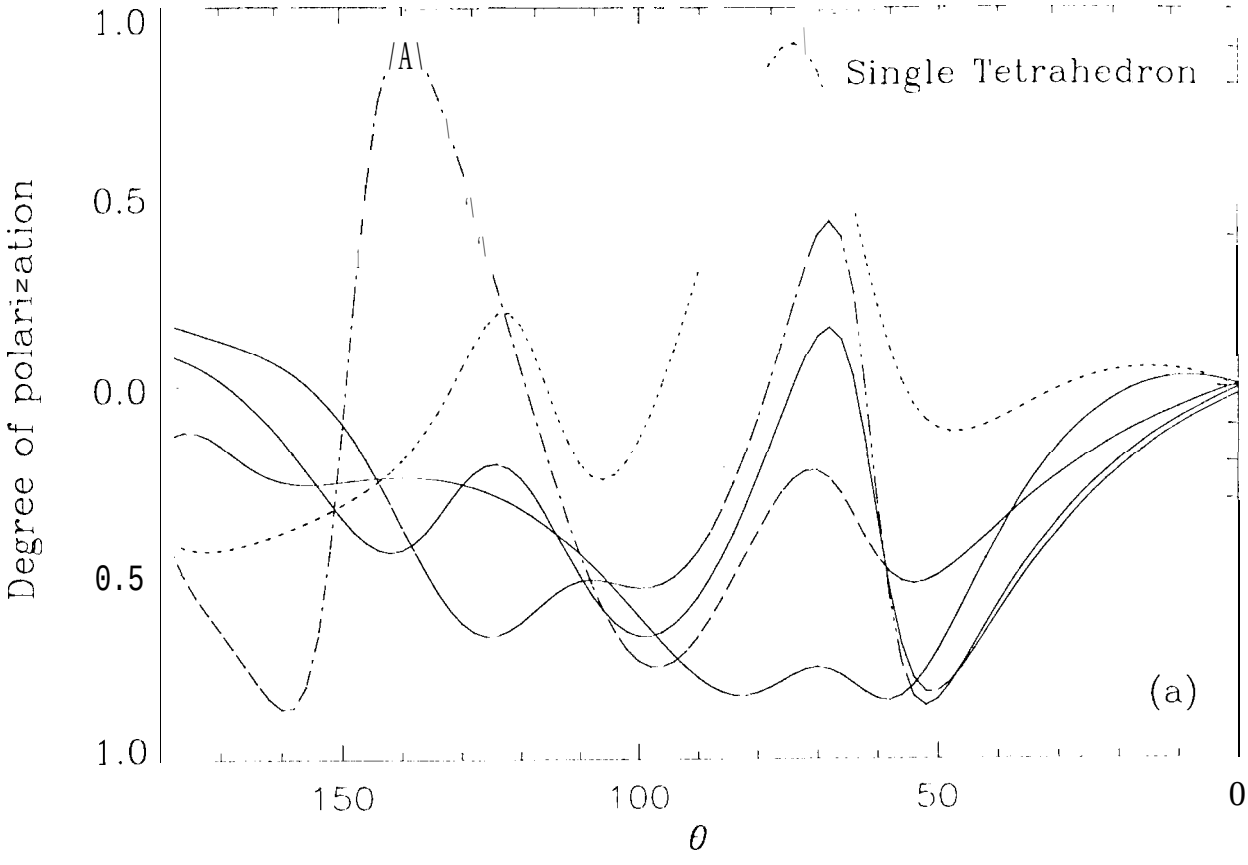
1.0
0.5
0.0
0.5
1.0
Degree of polarization
Single Tetrahedron
(a)
150
100
50
0
θ

Fig. 7 a,

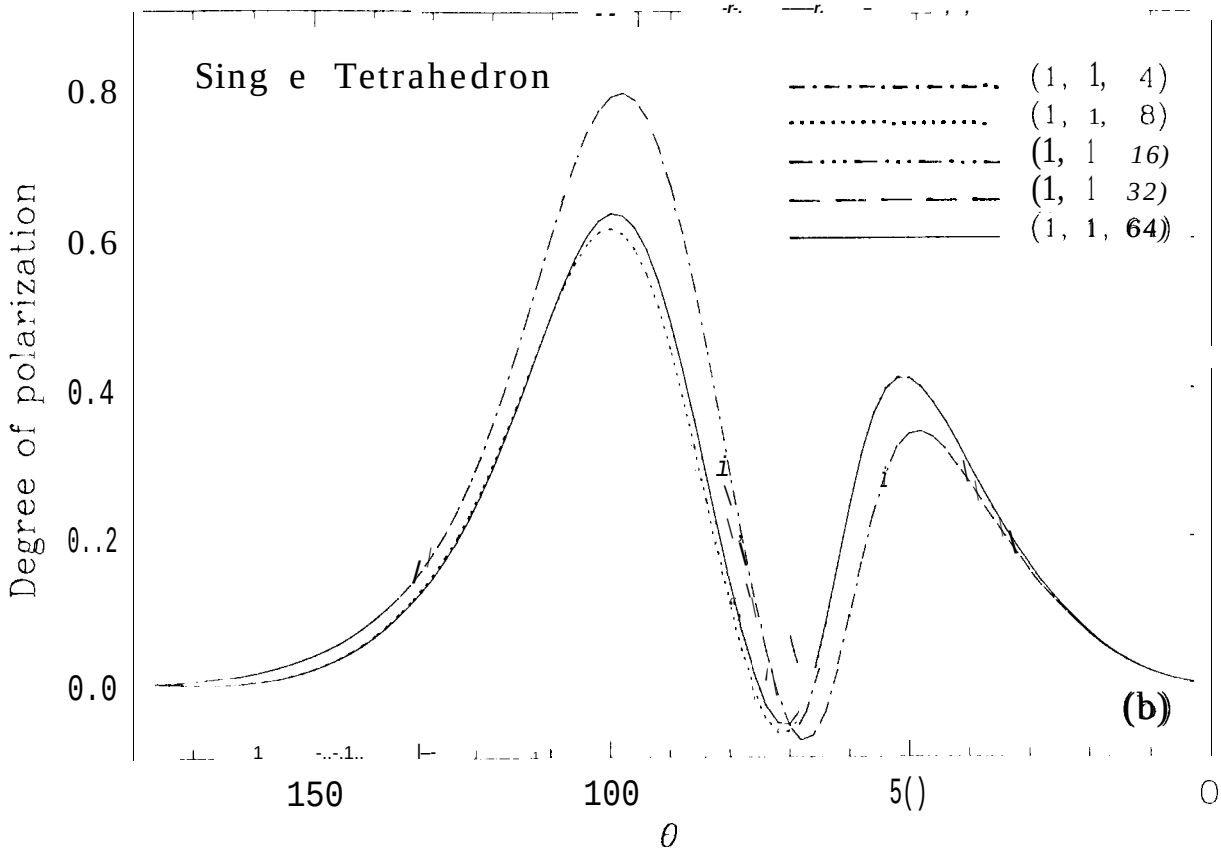
Sing e Tetrahedron
(1, 1, 4)
(1, 1, 8)
(1, 1 16)
(1, 1 32)
(1, 1, 64)
Degree of polarization
0.8
0.6
0.4
0..2
0.0
(b)
150
100
5()
0
θ

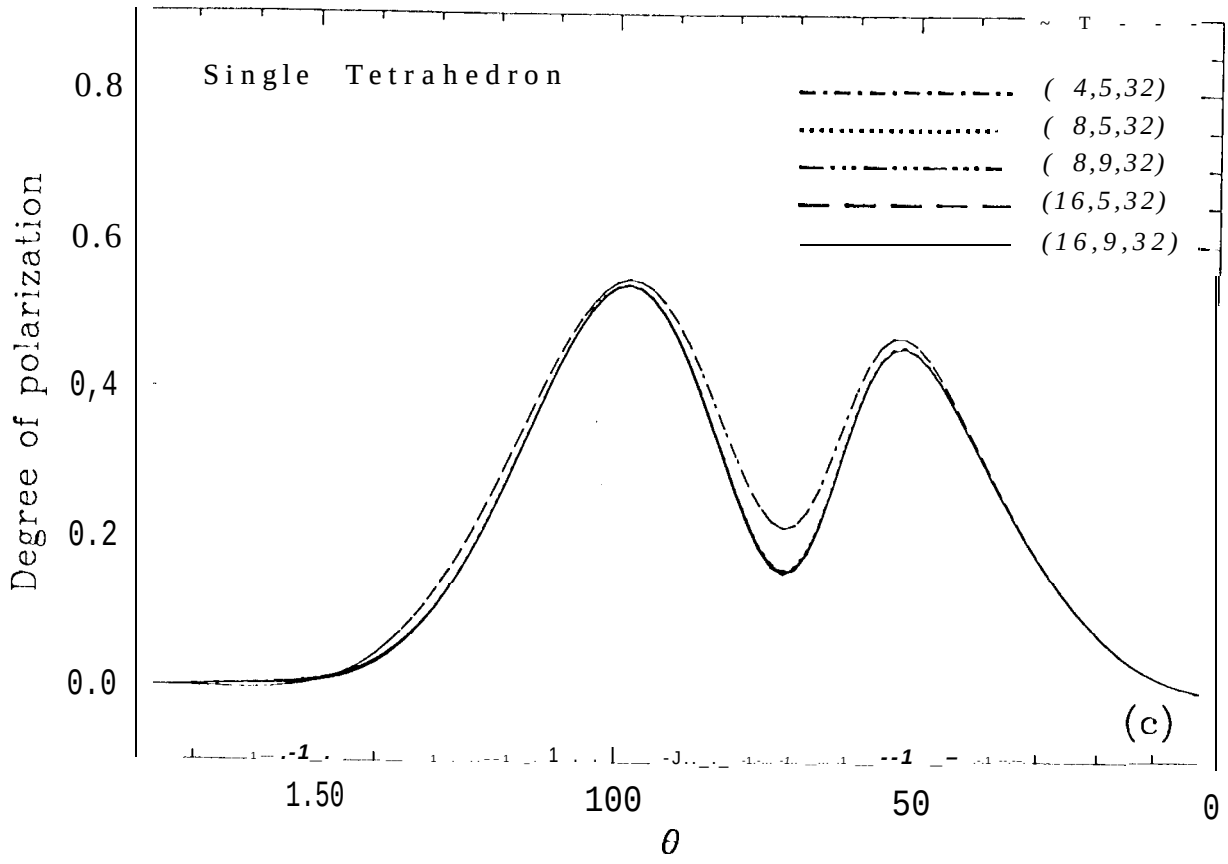
Single Tetrahedron
(4,5,32)
(8,5,32)
(8,9,32)
(16,5,32)
(16,9,32)
Degree of polarization
0.8
0.6
0,4
0.2
0.0
(c)
1.50
100
50
0
θ

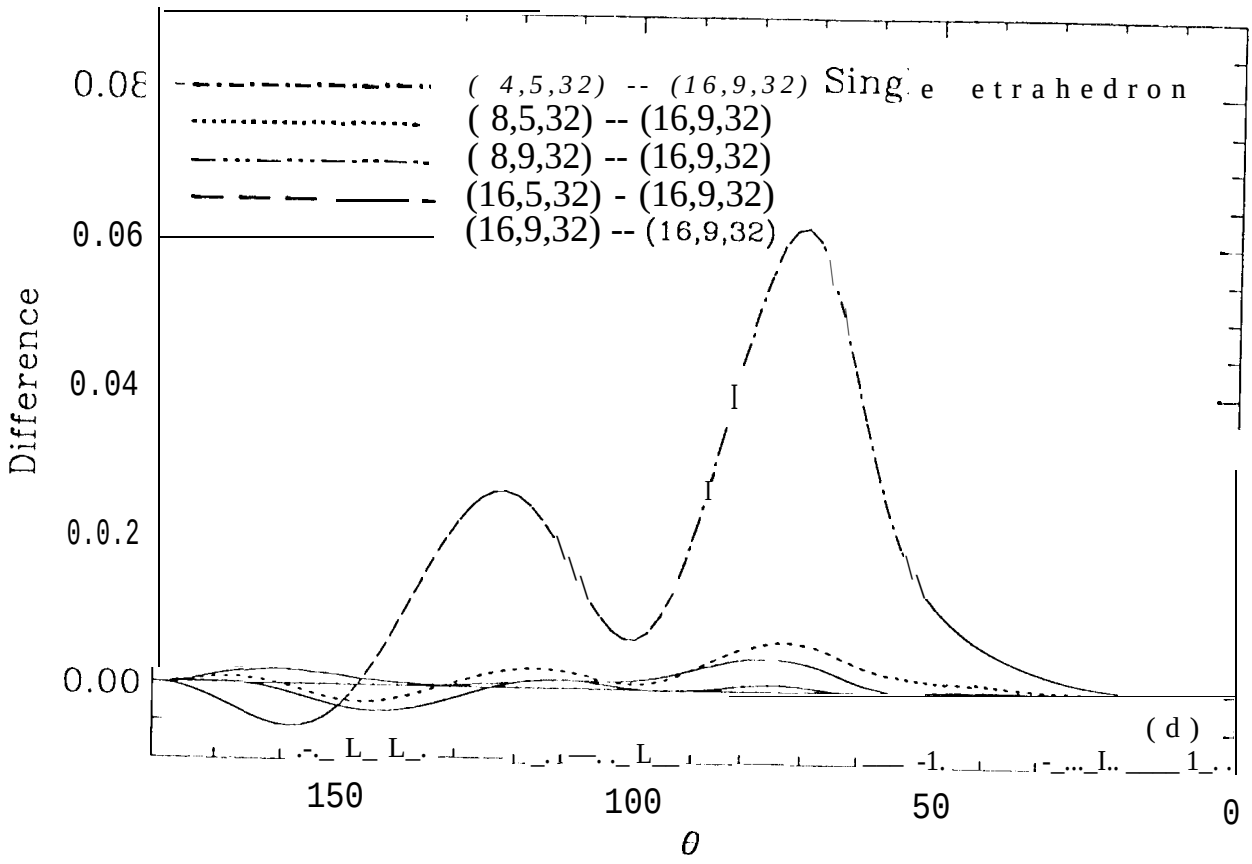
0.08
0.06
0.04
0.0.2
0.00
Difference
(4,5,32) -- (16,9,32) Single tetrahedron
(8,5,32) -- (16,9,32)
(8,9,32) -- (16,9,32)
(16,5,32) - (16,9,32)
(16,9,32) -- (16,9,32)
(d)
150
100
50
0
θ

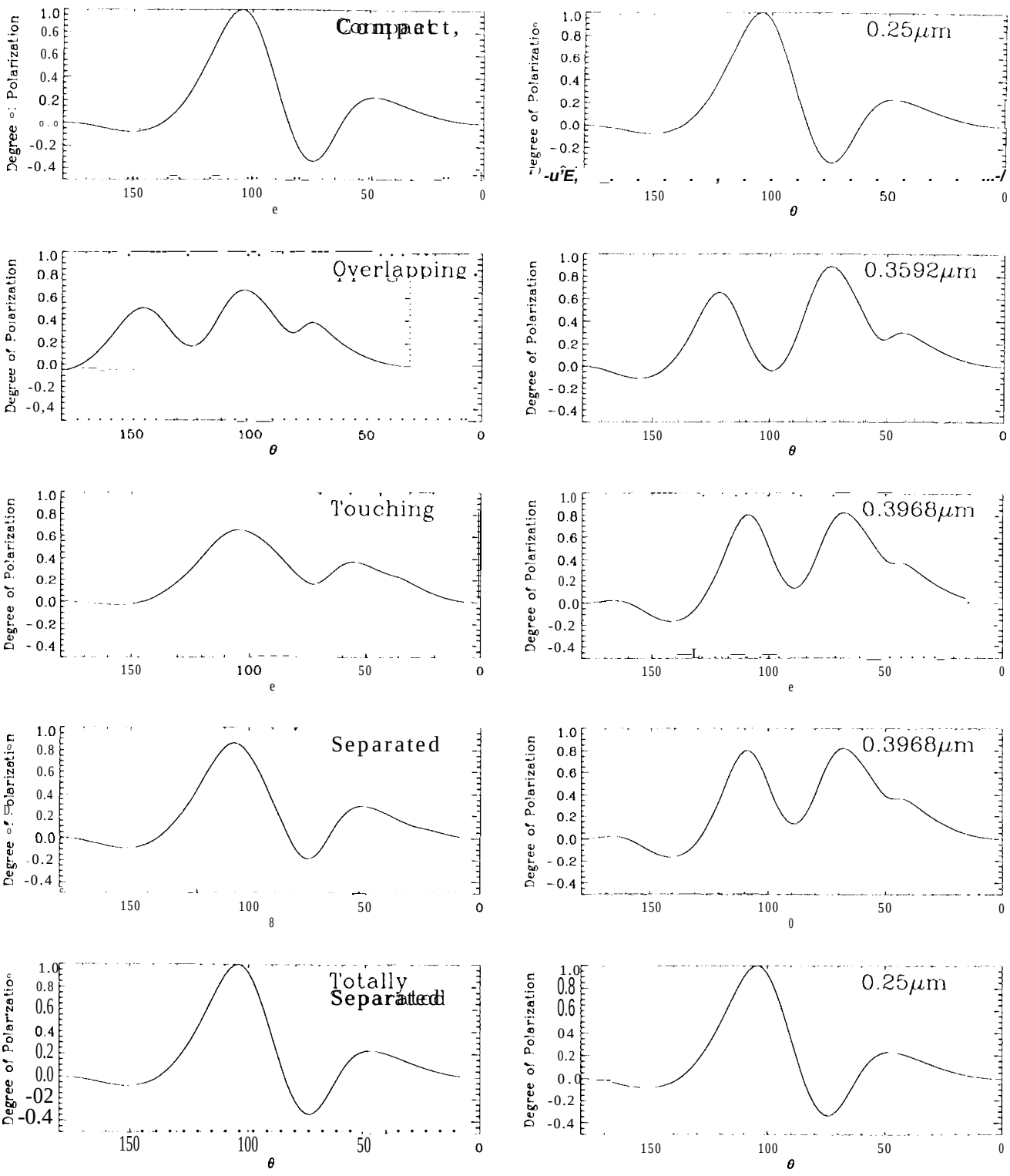
Compact,
0.25μm
Overlapping
0.3592μm
Touching
0.3968μm
Separated
0.3968μm
Totally Separated
0.25μm
Degree of Polarization
θ

Fig. 10

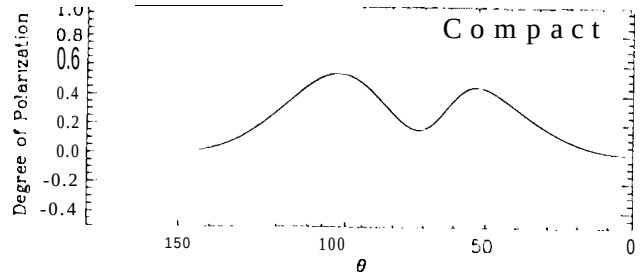
Compact
Degree of Polarization
θ

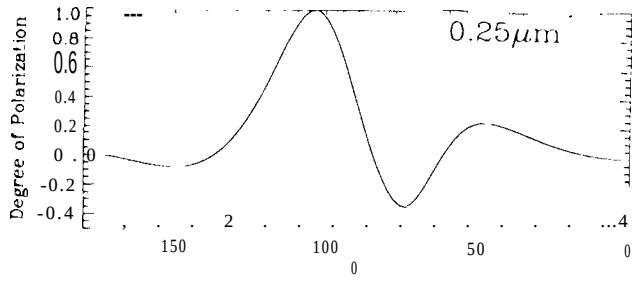
0.25μm
Degree of Polarization

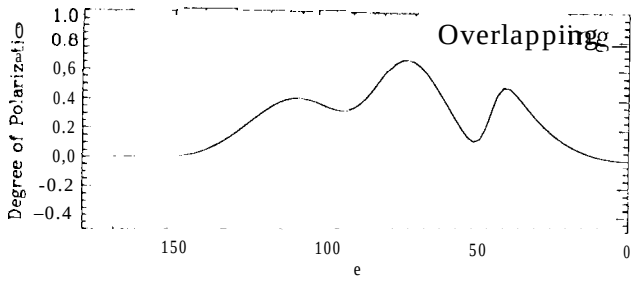
Overlapping
Degree of Polarization
e

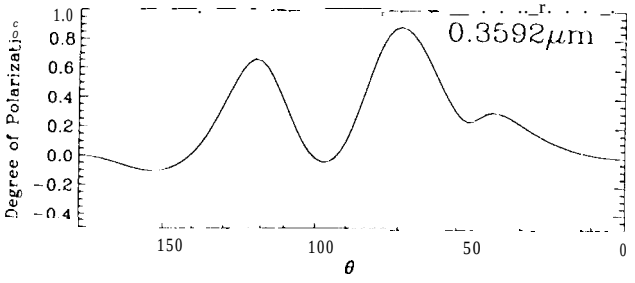
0.3592μm
Degree of Polarization
θ

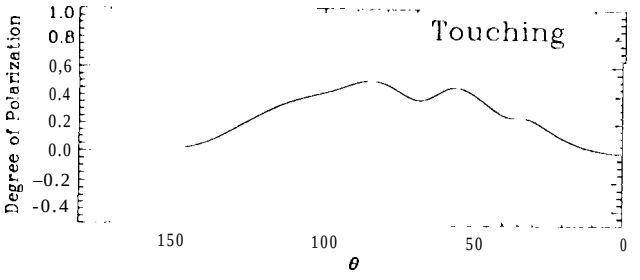
Touching
Degree of Polarization
θ

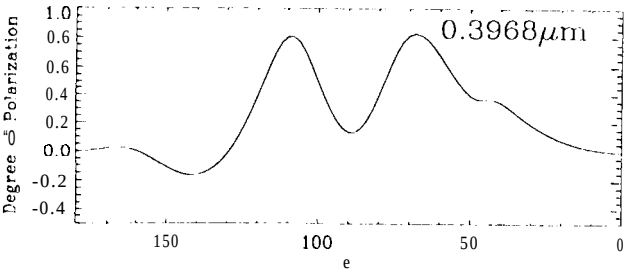
0.3968μm
Degree of Polarization
e

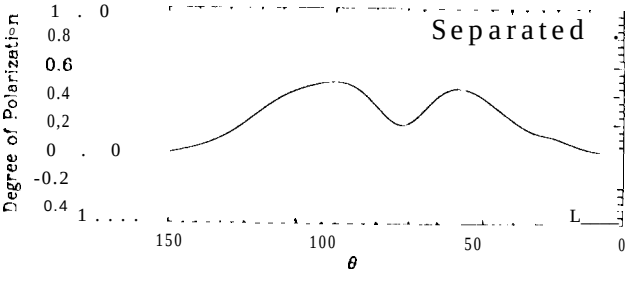
Separated
Degree of Polarization
θ

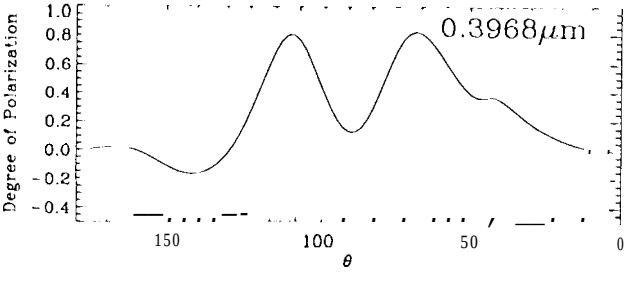
0.3968μm
Degree of Polarization
θ

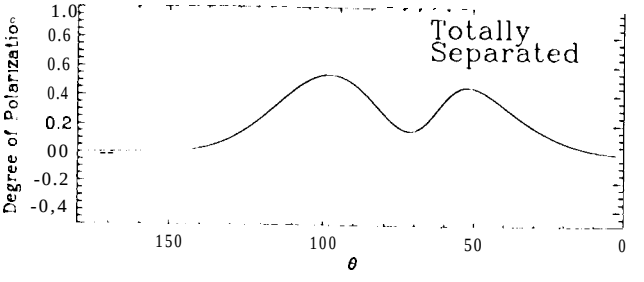
Totally
Separated
Degree of Polarization
θ

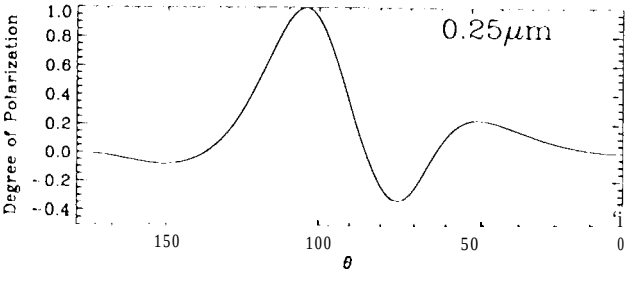
0.25μm
Degree of Polarization
θ

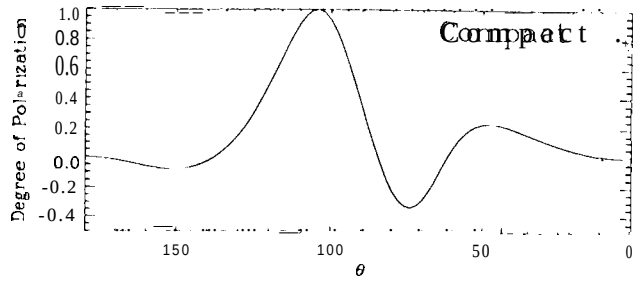
Compact
Degree of Polarization
θ

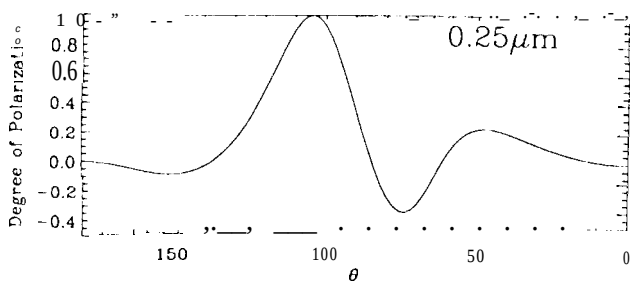
0.25μm
Degree of Polarization
θ

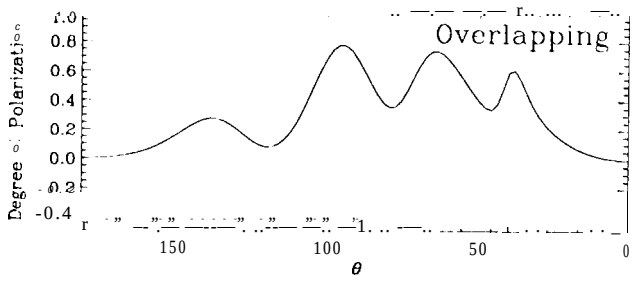
Overlapping
Degree of Polarization
θ

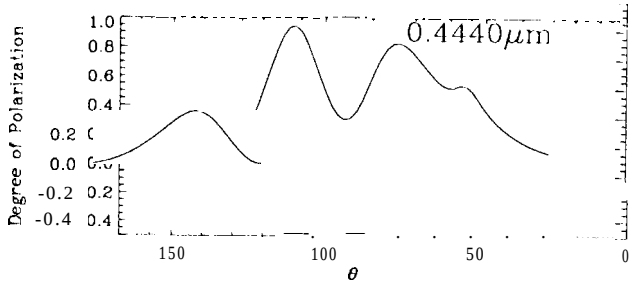
0.4440μm
Degree of Polarization
θ

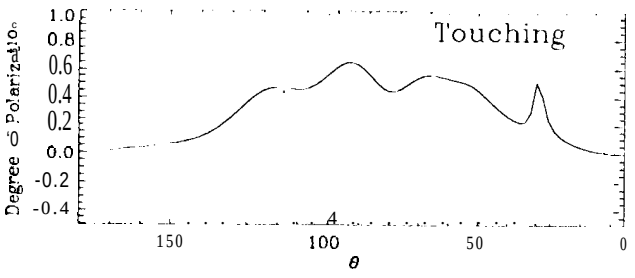
Touching
Degree of Polarization
θ

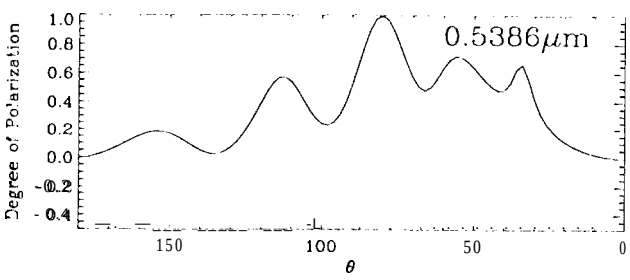
0.5386μm
Degree of Polarization
θ

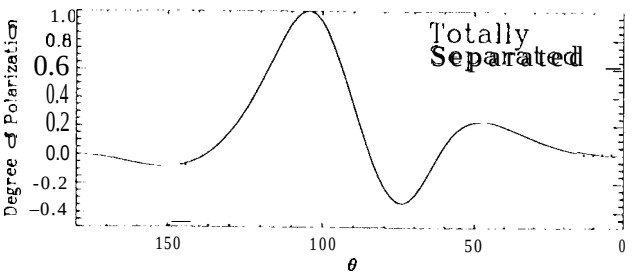
Totally
Separated
Degree of Polarization
θ

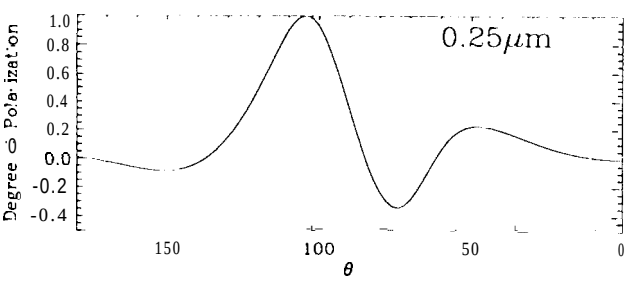
0.25μm
Degree of Polarization
θ

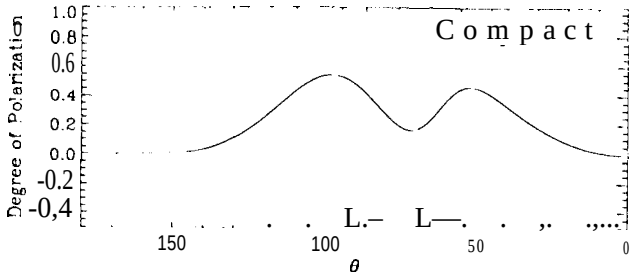
Compact
Degree of Polarization
1.0
0.8
0.6
0.4
0.2
0.0
-0.2
-0,4
150
100
50
0
θ

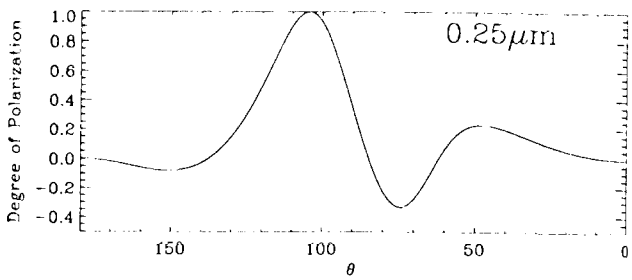
0.25μm
Degree of Polarization
1.0
0.8
0.6
0.4
0.2
0.0
-0.2
-0.4
150
100
50
0
θ

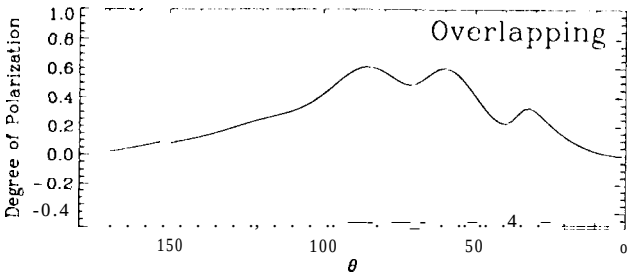
Overlapping
Degree of Polarization
1.0
0.8
0.6
0.4
0.2
0.0
-0.2
-0.4
150
100
50
0
θ

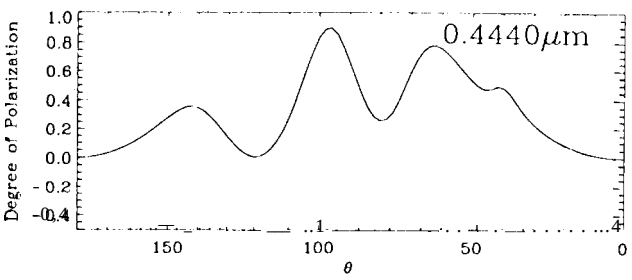
0.4440μm
Degree of Polarization
1.0
0.8
0.6
0.4
0.2
0.0
-0.2
-0.4
150
100
50
0
θ

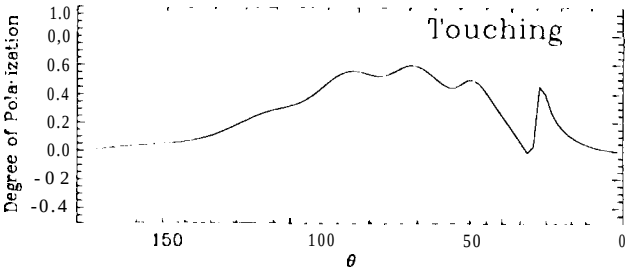
Touching
Degree of Polarization
1.0
0,0
0.6
0.4
0.2
0.0
-0.2
-0.4
150
100
50
0
θ

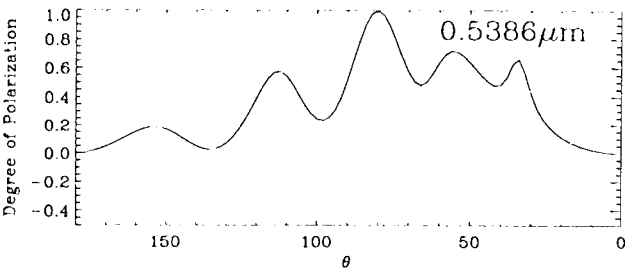
0.5386μm
Degree of Polarization
1.0
0.8
0.6
0.4
0.2
0.0
-0.2
-0.4
150
100
50
0
θ

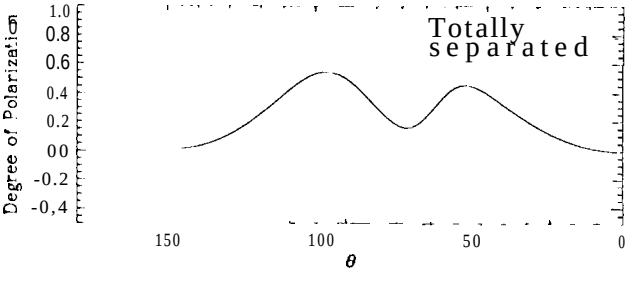
Totally
separated
Degree of Polarization
1.0
0.8
0.6
0.4
0.2
0.0
-0.2
-0,4
150
100
50
0
θ

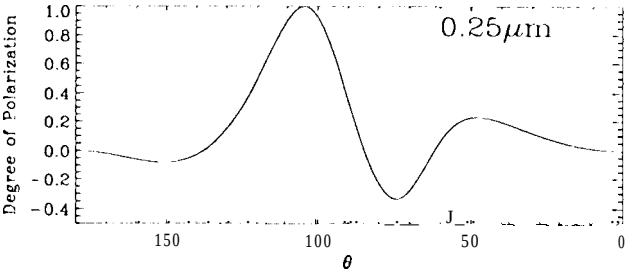
0.25μm
Degree of Polarization
1.0
0.8
0.6
0.4
0.2
0.0
-0.2
-0.4
150
100
50
0
θ

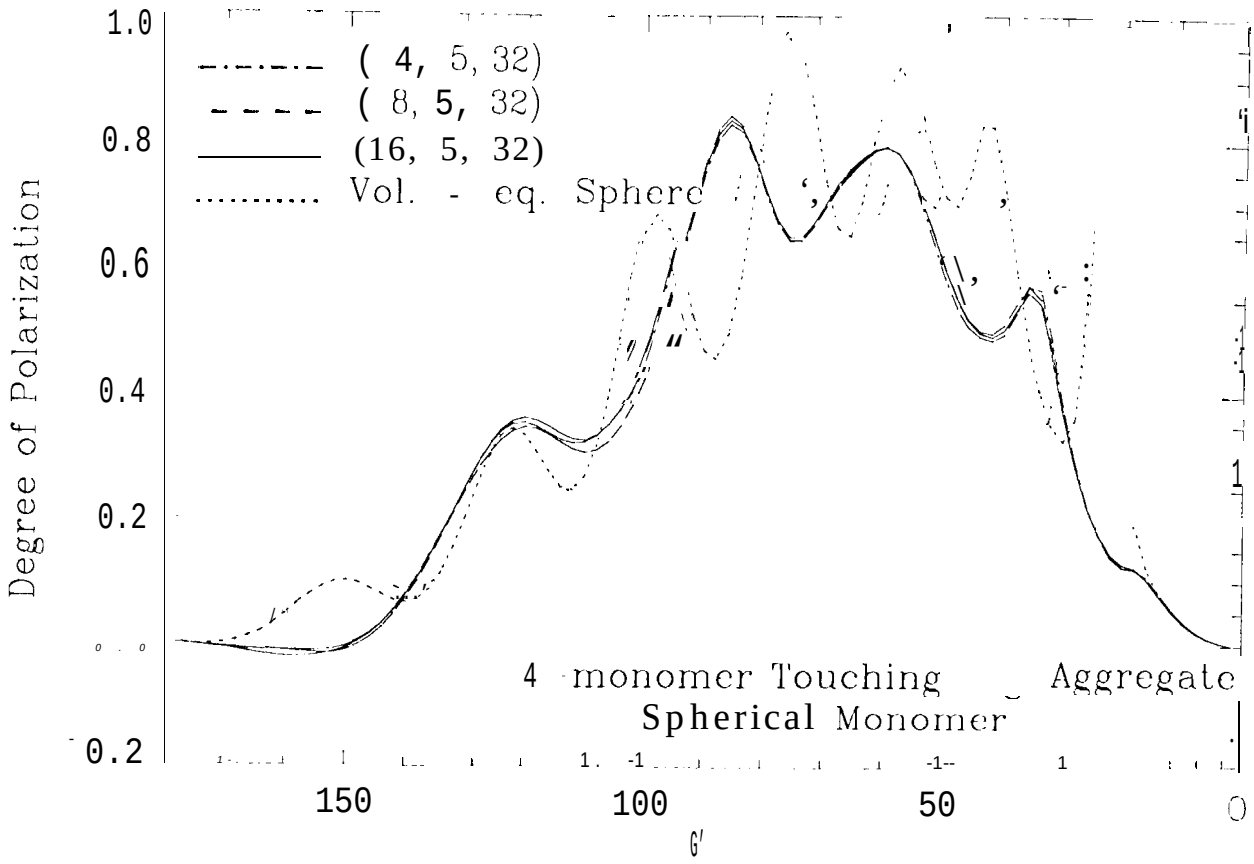
1.0
0.8
0.6
0.4
0.2
0.2
Degree of Polarization
(4, 5, 32)
(8, 5, 32)
(16, 5, 32)
Vol. - eq. Sphere
4 monomer Touching Aggregate
Spherical Monomer
150
100
50
0

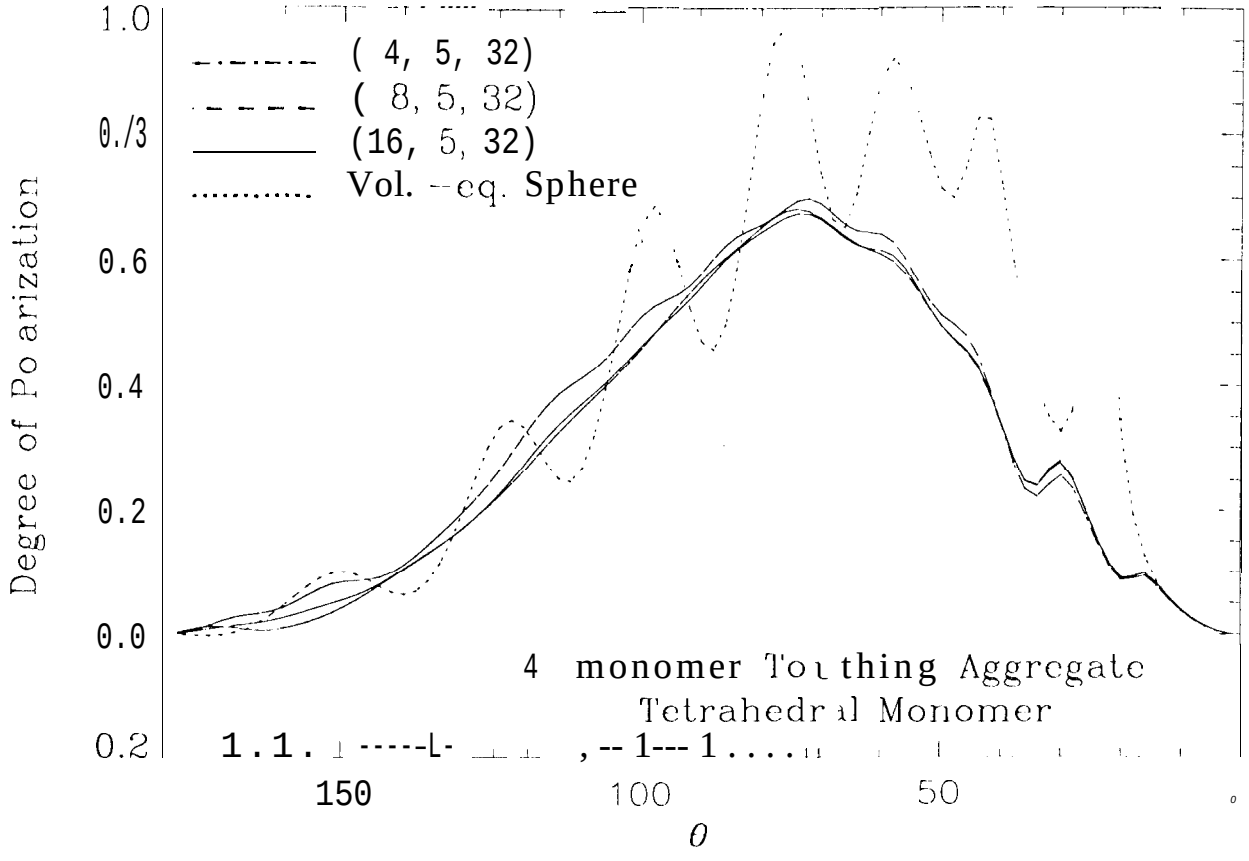
1.0
0./3
0.6
0.4
0.2
0.0
0.2
Degree of Polarization
(4, 5, 32)
(8, 5, 32)
(16, 5, 32)
Vol. -eq. Sphere
4 monomer Touching Aggregate
Tetrahedral Monomer
150
100
50
θ

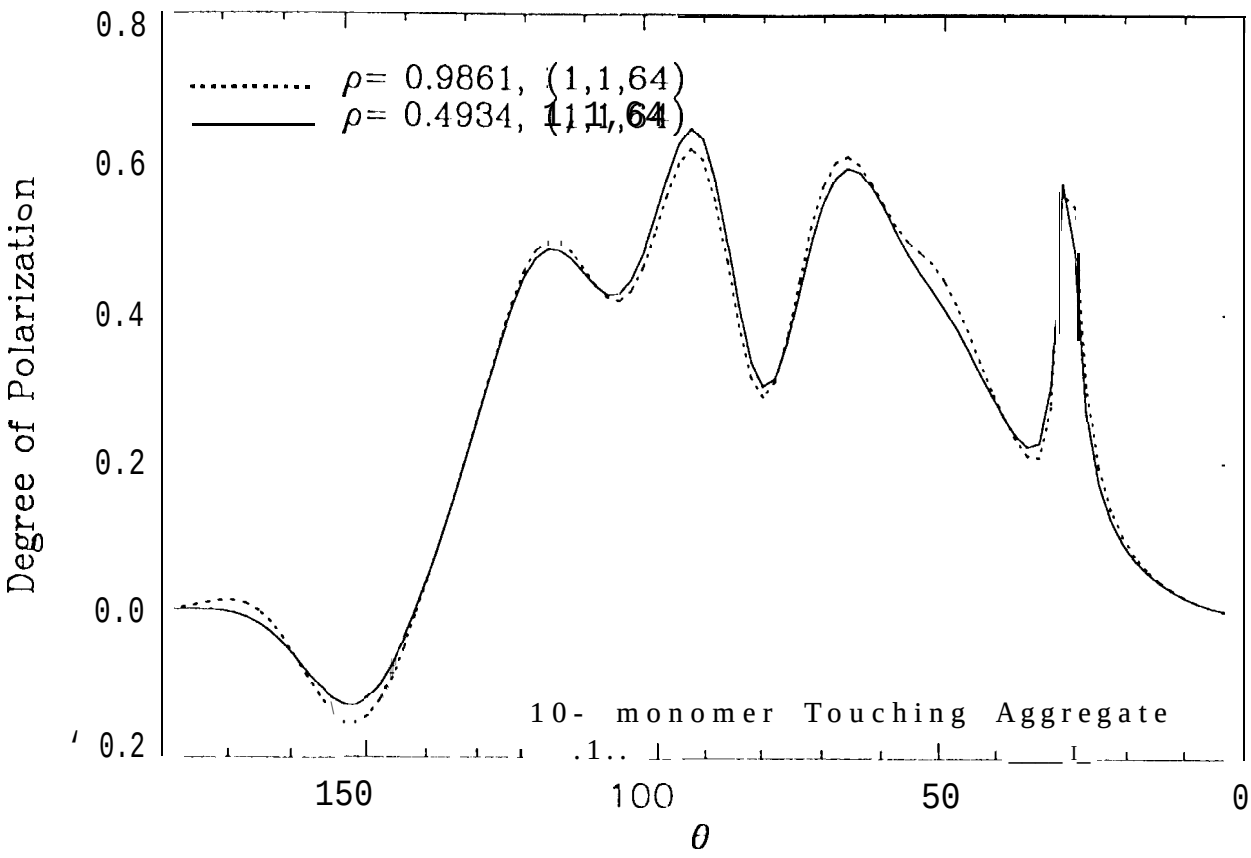
0.8
0.6
0.4
0.2
0.0
0.2
Degree of Polarization
ρ= 0.9861, (1,1,64)
ρ= 0.4934, (1,1,64)
10- monomer Touching Aggregate
150
100
50
0
θ

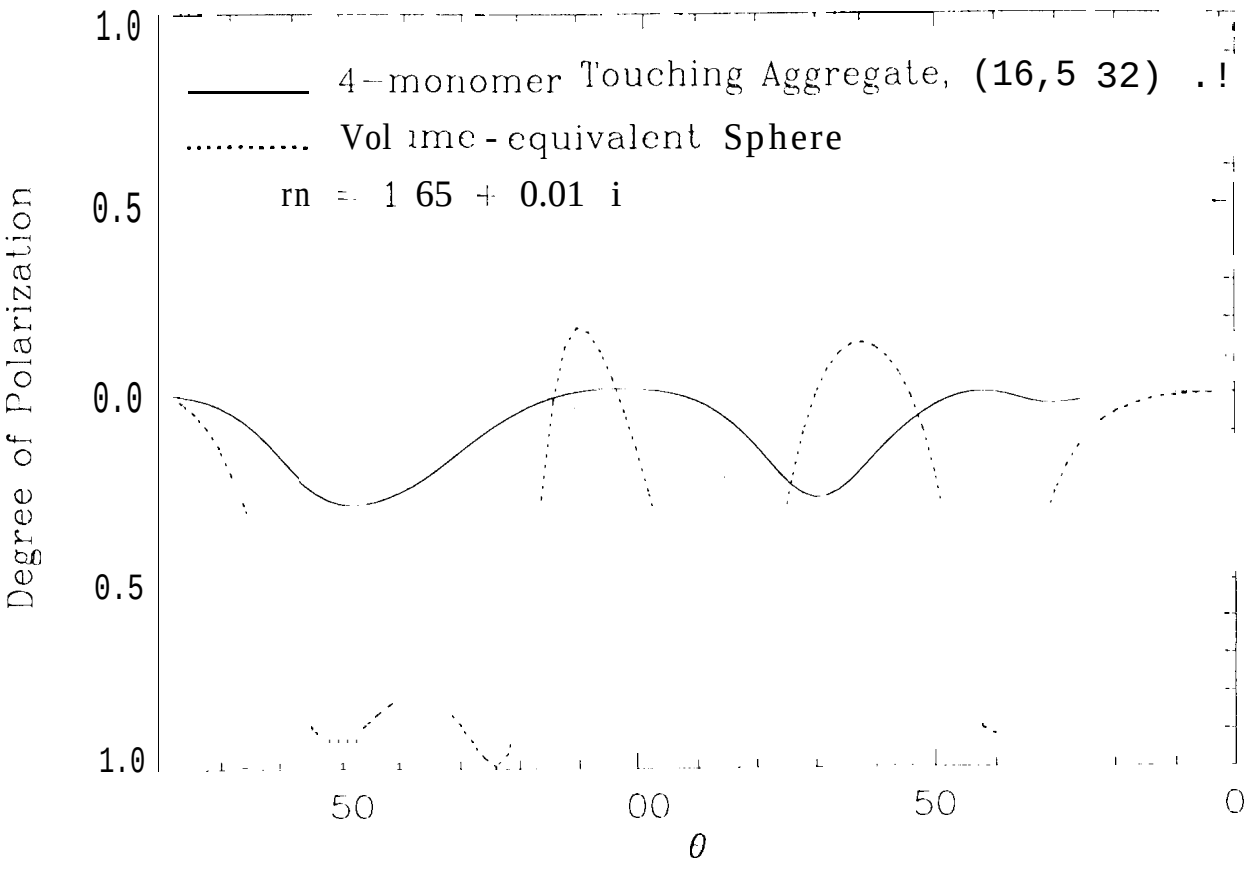
4-monomer Touching Aggregate, (16,5 32) .!
Vol ıme - equivalent Sphere
rn = 1 65 + 0.01 i
Degree of Polarization
1.0
0.5
0.0
0.5
1.0
50
00
50
0
0

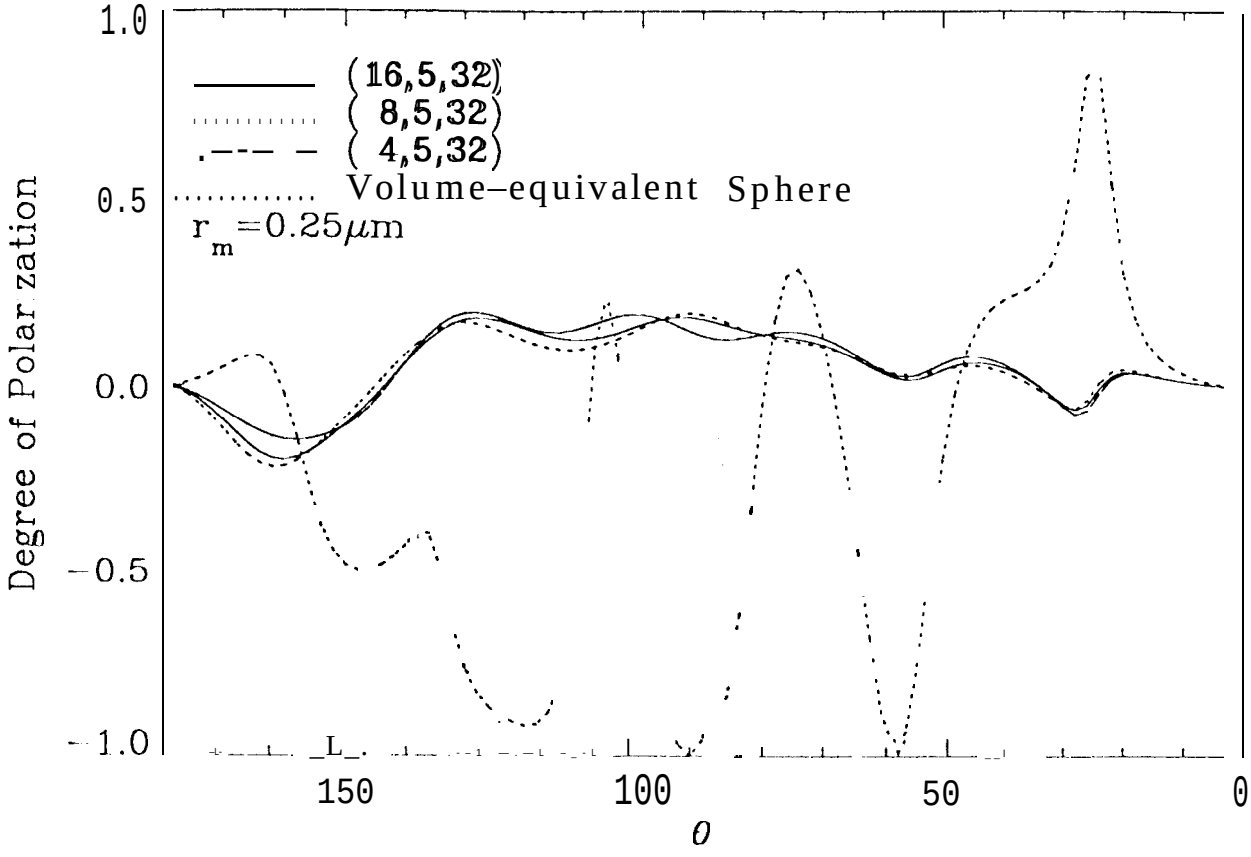
1.0
0.5
0.0
−0.5
−1.0
Degree of Polarization
(16,5,32)
(8,5,32)
(4,5,32)
Volume–equivalent Sphere
$r_m = 0.25\mu m$
150
100
50
0
θ

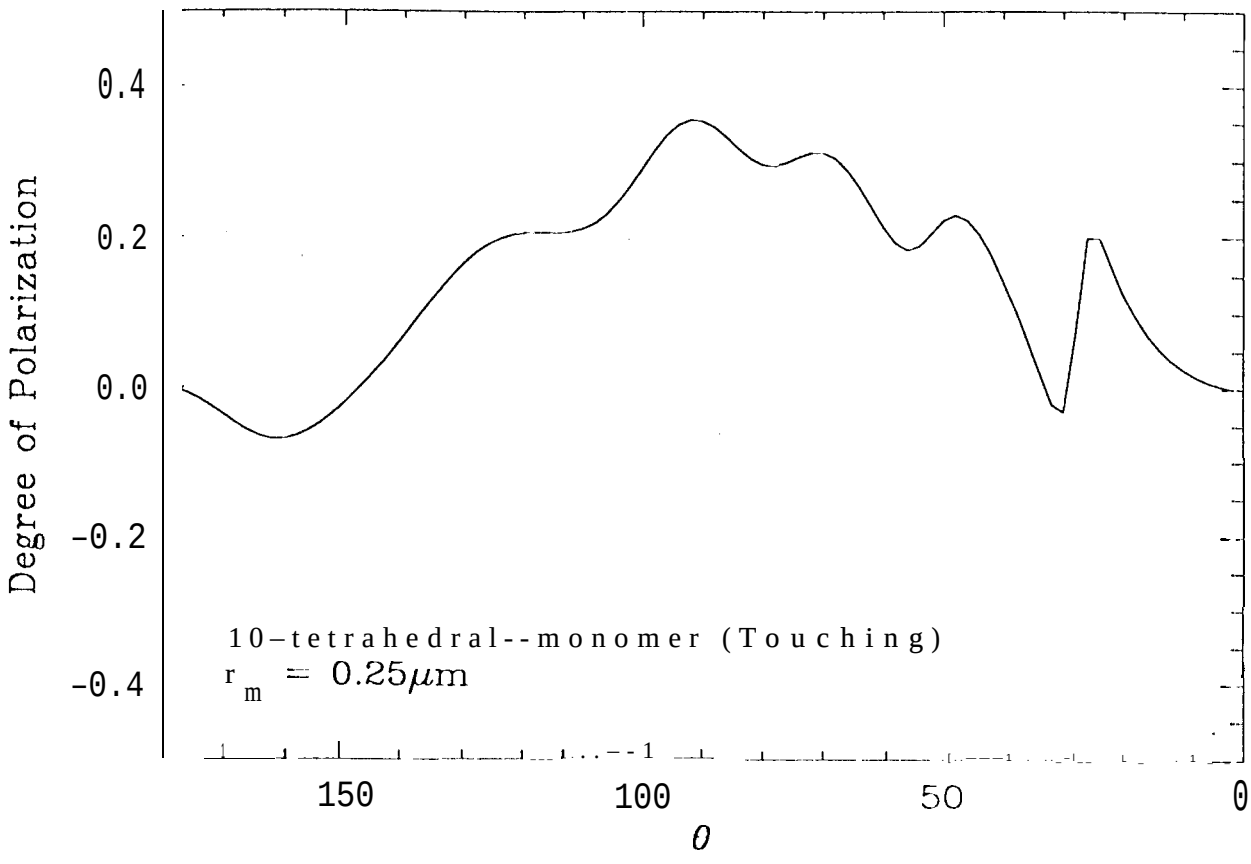
0.4
0.2
0.0
-0.2
-0.4
Degree of Polarization
10-tetrahedral--monomer (Touching)
r m = 0.25μm
150
100
50
0
θ

4–monomer Aggregate

10–monomer Aggregate

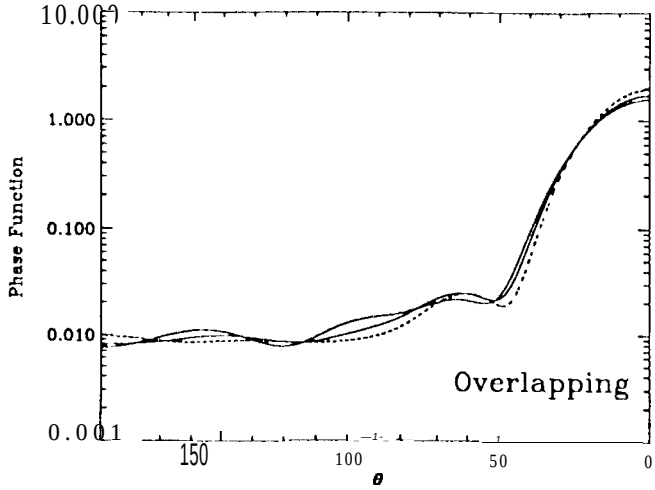

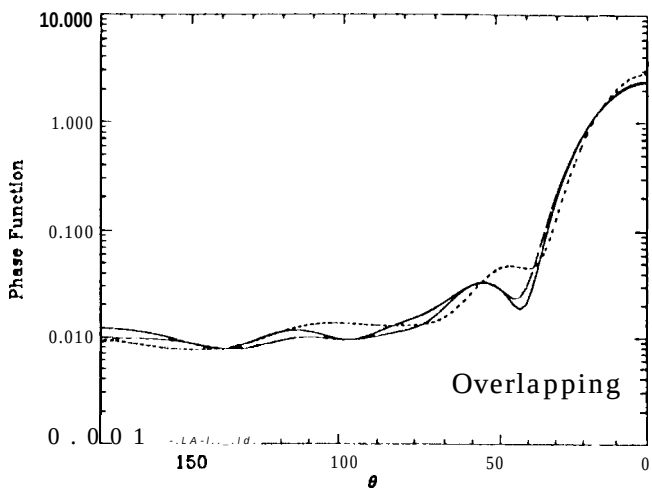

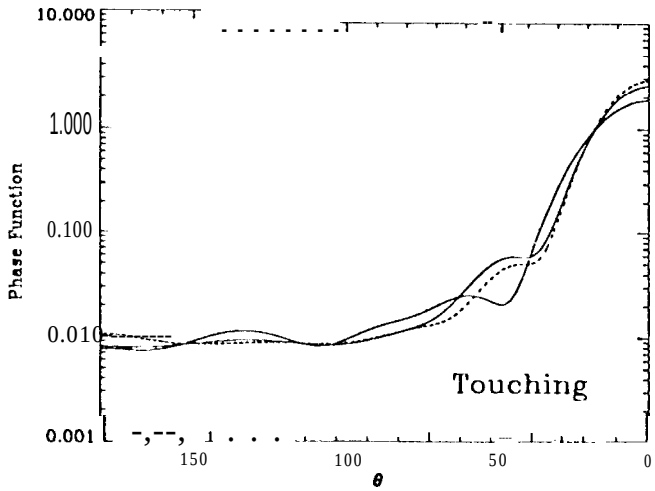

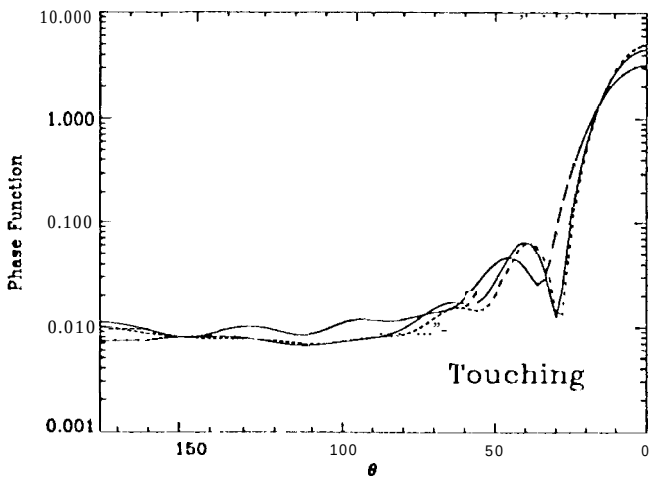

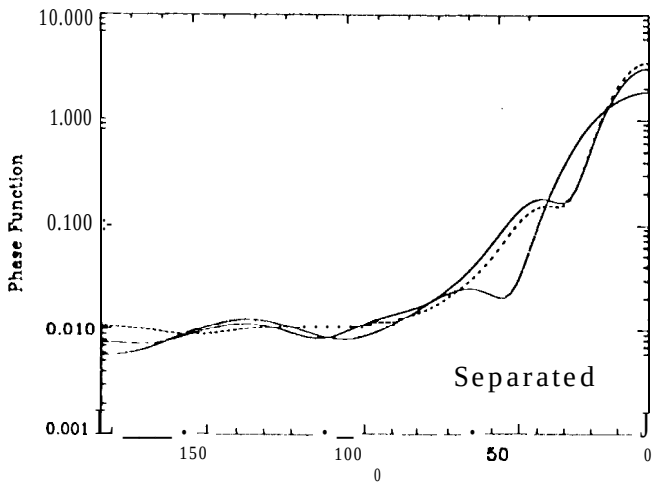

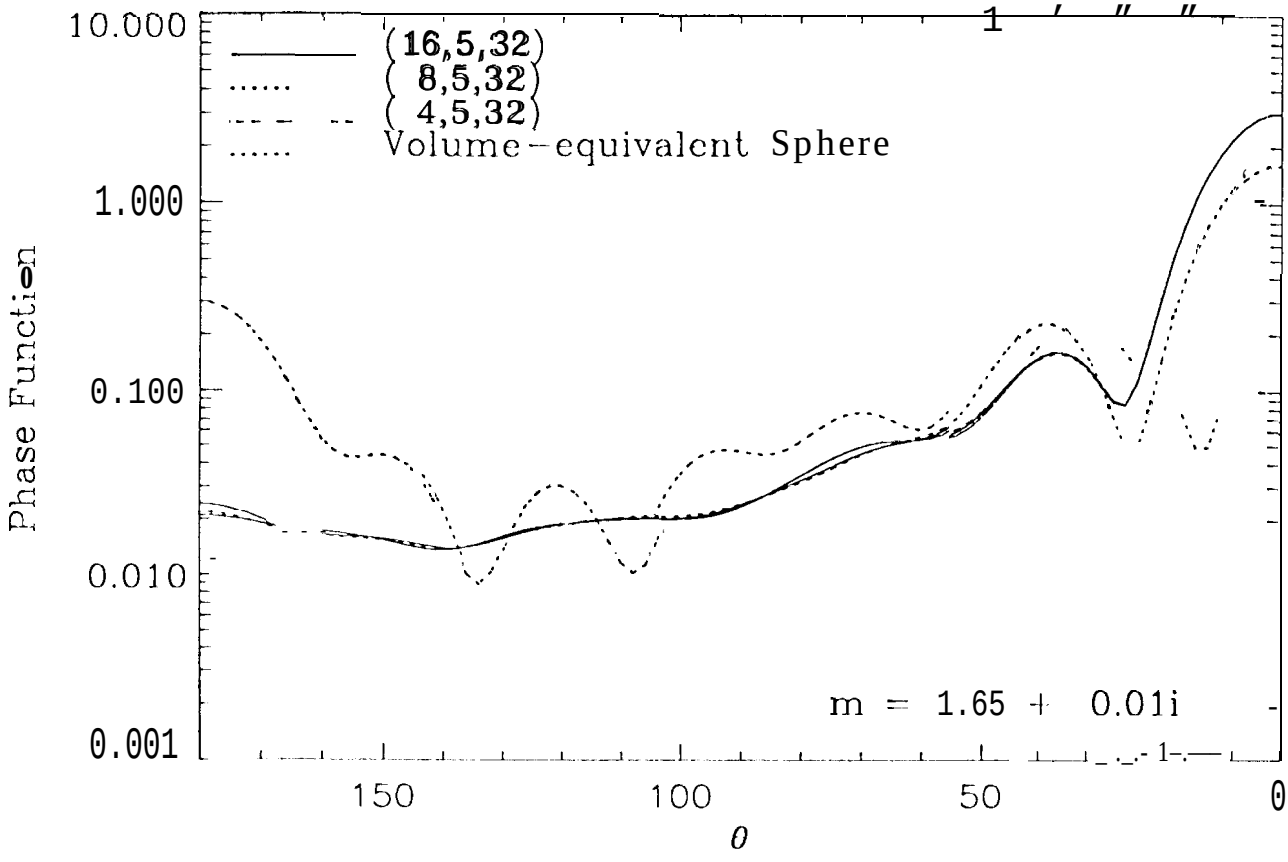
10.000
1.000
0.100
0.010
0.001
Phase Function
(16,5,32)
(8,5,32)
(4,5,32)
Volume-equivalent Sphere
m = 1.65 + 0.01i
150
100
50
0
θ

Fig. 5

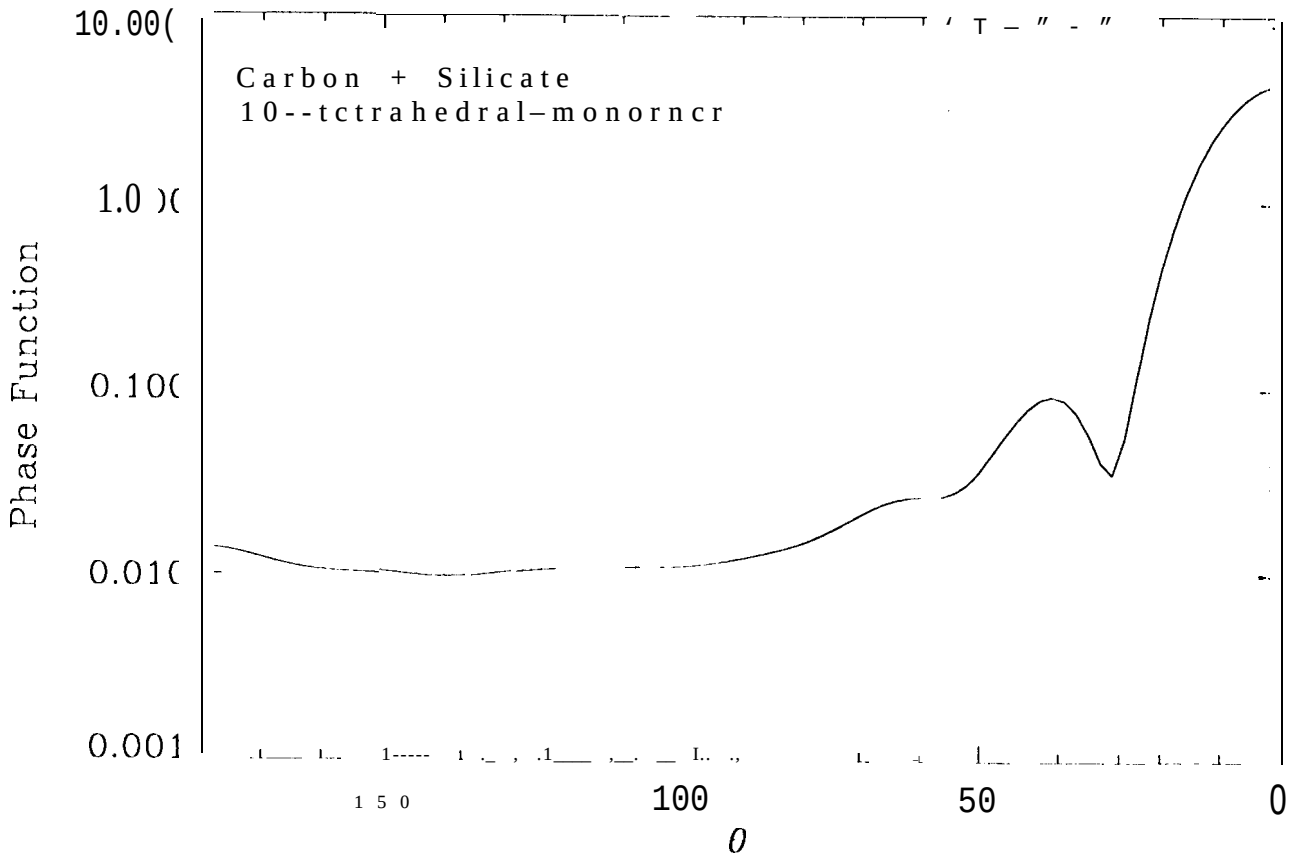
Carbon + Silicate
10--tctrahedral–monorncr
Phase Function
10.00(
1.0)(
0.10(
0.01(
0.001
150
100
50
0
0